2009

# An Idealized Model and Systematic Process Study of Oxygen Depletion in Highly Turbid Estuaries

Stefan A. Talke
*Portland State University*, talke@pdx.edu

Huib E. de Swart
*Utrecht University*

Victor de Jonge
*University of Hull*

Editorial Manager(tm) for Estuaries and Coasts
Manuscript Draft

Manuscript Number: ESCO-D-08-00110R1

Title: An idealized model and systematic process study of oxygen depletion in highly turbid estuaries

Article Type: Original Report

Keywords: Estuarine circulation, Estuarine Turbidity Maximum, Suspended Sediment Dynamics, Morphology, Fluid Mud, Water Quality, Hypoxia, Anoxia, Ems Estuary

Corresponding Author: Stefan Talke,

Corresponding Author's Institution: University of Washington

First Author: Stefan A Talke, PhD

Order of Authors: Stefan A Talke, PhD; Huib E de Swart , PhD; Victor de Jonge, PhD

Feb 17, 2009

Dear editors,

Please find enclosed a revised version of the manuscript titled “An idealized model and systematic process study of oxygen depletion in highly turbid estuaries”, ESCO-D-08-00110, by Talke, De Swart and De Jonge. We are also including an additional 3 files, which we would like to publish as supplementary material.

The products are the result of a labor-intensive process in which we made a more thorough analysis of field data, calibrated model results to the field data, re-organized the main text, simplified the figures and presentation, and shifted parts (such as complete sensitivity studies) to the supplementary material. We believe that these changes, which were made in response to editor and reviewer comments, have bolstered both our results and our presentation. The supplementary material contains supporting material for readers who would like more background information, while the main text is now focused towards the broader Estuaries and Coasts audience.

Yours sincerely,

(also on behalf of H.E. de Swart and V.N. de Jonge),

Dr. S.A. Talke

***Response to Reviewer Comments**

*Feb. 17, 2009*

*Dear editors and reviewers,*

*In the following pages, our responses to the comments of the editors and reviewers are given in italics. We thank the editors and the reviewers, and believe the manuscript has been much improved by your constructive comments.*

*Yours sincerely,*

*(also on behalf of H.E. de Swart and V.N. de Jonge),*

*Dr. S.A. Talke*

**Detailed Reply to Editor**

Comment: I ask that you give particular attention to these weaknesses in the current manuscript: (a)absence of explicit statements and justifications of all assumptions (both implicit and explicit); (b) absence of derivation and justification of equations comprising your model; and (c) absence of any verification of model computations through comparisons against measurements.

*To address these major comments, we have*

- *(a) Produced a figure (Fig 6) which portrays the geometric configuration of the model and the key assumptions made during the derivation*
- *(b) Included a complete derivation of the circulation and SSC model in an electronic supplement (supplement S.1). In addition, we have added data and discussion into Supplement S.2 which justifies our diagnostic model of salinity and the functional form of the vertical variation in SSC. We have also included more references to Talke et al. (2008,2009), which also describe the model, in the main text.*
- *(c) Explicitly compared the results of our DO model with measurements from 3 stations in the Ems estuary in Section 4.1 (labeled 'Model validation'). Fig. 7 now shows a comparison of DO vs. SSC (modeled and measured) and Fig. 8 now shows a comparison of measured and modeled DO as a function of temperature. In addition, we have reconfigured our experimental results section to show more clearly the longitudinal structure of SSC and DO, as well as the historical changes to these over the past 2 decades. Establishing these facts more explicitly allows for better comparison with the results of the estuarine DO model.*

Comment: Your manuscript is long, a bit tedious to read, and therefore will not attract the attention it deserves from busy readers. This problem can be resolved if you restructure your paper so the modeling details (e.g. sensitivity analyses and associated figures) are placed in a document that will be archived as online Supporting material.

*To address this comment, we have reconfigured the results section. Section 4.1 has been reconfigured to become a 'model validation' section, as requested by the reviewers. To streamline the model results presentation, Eq. 17-19 and its development and discussion have been placed into section 3.2. Eq. 20, the former Fig. 6, and much of the associated discussion from the former section 4.1, have been placed in Supplement S3. This has removed about 930 words.*

*In Section 4.2, Figures 8-10 and Figs. 12-13, and the associated text describing these sensitivity studies, have been moved to Supplement S.3. Approximately 1800 words of text were removed in this way.*

*In the place of the exhaustive sensitivity studies we have included figures that (a) explain the effect of known changes that have occurred to the estuary and/or (b) demonstrate a critical*

*sensitivity. These figures are now simplified and shown as pcolor plots, which allows for more accessible reading and interpretation.*

Comment: Then, you can focus your manuscript on the key results so they will be more accessible to general readers. In the end, your primary text can be greatly streamlined by focusing on model justification and results that will of general interest, and then archiving the modeling details for the smaller audience of scientists/engineers who will be interested in those details.

*We have archived material into 3 Supplemental sections, and believe the main text is now much more focused on the key results.*

Comment: Finally, please compose a new Abstract, following guidelines to authors specifying a concise abstract of 100-150 words.

*We have written a new abstract that is 150 words long.*

**Detailed reply to Associate Editor**

Comment: The ms tried to combine three aspects: a. presents the fact that SSC and hypoxia are closely related in a highly turbid river (so that DO consumption is a function of SSC); b. derivation of a DO model, based on their previously-derived momentum-SSC model; and c. model results and sensitivity tests against choices of parameters.

In part b, assumptions and derivations leading to Eq. 5 was not clearly stated. I understand that this was included in another paper (Talke et al., 2009). But all assumptions need to be clearly listed perhaps using a table (salinity vertically well-mixed; horizontal salinity distribution was presumed as a known function so that flow field and salinity distribution is not solved as a coupling process; vertical distributions of SSC and DO was solved, again, from decoupling them with the horizontal flow field, etc) and when Eq. 5 was given, a reference should be added.

*The major assumptions have been included in the new Fig. 6, and we have included more references to Talke et al., (2008,2009). We have also included a more thorough derivation of the circulation and SSC model in Supplement S1.*

Comment: In part c, I'd suggest the authors to include some real-case data in discussing the model results. For example, the authors have excused channel deepening from 5 to 7m as one of the primary cause for higher frequency of hypoxic events in the Ems estuary, some averaged DO concentrations before and after channel deepening could be added to figure 6c.

*We have addressed this comment by adding Fig. 4 and Fig. 5 to the field-results section (which show DO concentrations as a function of salinity before and after deepening from 5 to 7 m), and Fig. 7 and Fig. 8 to the results section (which explicitly compare measured and modeled DO as a function of SSC and temperature).*

*Fig. 4 and Fig. 5 explicitly establish the DO concentrations as a function of salinity before and after deepening, and link worsening DO conditions to changes to the turbidity zone (0.5- 2 psu salinity). This conclusion allows us to better compare field results with the results of our model study (Fig. 9), though explicit comparisons are not possible because SSC data is unavailable before 1998.*

*Fig. 7 and Fig. 8 explicitly compare model and measurement results, hence addressing the comment about including real case data into discussion of the model.*

Several assumptions adopted by the model may lead to DO prediction being vertically over-mixed. For example, the assumption of well-mixed salinity field and the independent solution of vertical TSS and DO concentrations from the impact of residual circulation. The limitations of the model and the restrictions of its application because of the assumptions need to be better discussed.

*The model assumptions can now be seen in Fig. 6, and more in-depth discussion of the model derivation and assumptions are given in Supplement S.1. We use scaling to show in Supplement S.1 that residual circulation is a higher order effect on the distribution of SSC. Residual*

*circulation and dispersion do affect the DO model, as can be seen by the slight variation between DO minimum and SSC maximum in some of the results.*

*Finally, we also acknowledge the limitations of the model in the discussion more clearly with this sentence: "As discussed in more detail in Talke et al., (2009), the tidal averaged model of circulation and SSC distribution neglects tidally varying processes (e.g., settling lag, periodic salinity stratification, etc) that influence tidally averaged circulation and the fluxes of sediment in an estuary"*

**Detailed reply to Reviewer #1**

My main concern however is that the model solution of the flow field is not provided. Equation (5) needs to be derived clearly, or a reference used, and proper discussion about its applicability given. The flow field is one of the most important ingredients of the driving force. Therefore, I suggest that the authors add this part in their revision.

*We appreciate the reviewers comment, and agree that Eq. 5 was introduced rather abruptly. We know have included the requested reference and have included a derivation in the supplemental section S.1. An expanded discussion of assumptions has also been included.*

I would like to have enough information to evaluate the applicability of this model. I do have my doubt about the applicability to an exponentially decreasing channel. But that doesn't necessarily suggest in anyway a negative review. It is also important that the authors think through on this issue and make sure the solution is correct for the channel they used (equation (1) for the channel width). I look forward to reading the revision.

*The more in-depth derivation of the model in supplement S.1 as well as references to Talke et al., 2007b address this comment. Exponential models are often used in idealized models, and we have added a reference to Eq. 1 to justify its use.*

Detailed comments:

1. Page 1, line 21, the last "in" should be deleted

*We have made the requested change*

2. Page 3, line 59, Humber Estuary, Loire Estuary, Yellow River Estuary
   *We have made the requested change.*

3. Page 3, line 62, delete "observed and modeled"
   *We have made the requested change.*

4. Page 4, line 79, define SSC first (the definition on the next page in line 106 should be moved to here.
   *We have made the requested change.*

5. Line 80, what do you mean by "fast"? Fast in calculation?

*We have made the description more clear.*

6. Line 93, specify what does it mean by "well mixed": vertically, horizontally?

*We added the qualifier "vertically" to this sentence.*

7. Figure 1, can you just use grayscale for the map? The colors are kind of odd.

*We have made the requested change*

8.Line 131, talking about the ebbing and flooding phase observations, can you first describe the tidal conditions there, rather than just specifying the tidal range being mesotidal? Is it semi-diurnal, mixed, diurnal?

*We've added the requested information about the tides, and removed the description 'mesotidal', since this was redundant with the reported tidal range.*

9. The observations were not conducted instantaneously. Can you describe the observations a little more, e.g. How long did it take to run the ~ 50 km length transect? How long did that take in reference to one tidal period? Figures 3 and 4 show results from "ebb" and "flood" phases, but here the words "ebb" and "flood" are vague as running along a 50 km transect with water sampling, CTD casts etc will require extended length of time. That time may cover partial ebb and partial flood tide phases, or any period in between. It is therefore important to indicate (e.g. with a figure) the time segments. This may not appear to be a big problem when Figures 3a and Figure 4a are compared: they appear to be almost identical, suggesting that the ebb and flood conditions were quite similar. Figures 3b and 4b however do show some differences. This is a little bit surprising. But this also highlights the need to describe the observations in more details to avoid confusion.

*We thank the reviewer for this observation, which is indeed pertinent for interpreting the data. We have added a brief discussion of the tidal phases of the measurements to the discussion of these two figures (now Fig. 2 and Fig. 3), both in the text and in the figure captions. We also reference Talke et al., 2009, which discusses these measurements as well.*

10. The last statement at the end of page 6 and the top of page 7 is not quite convincing to me. The local minima is ~ 2, which can be found elsewhere in the figures, not just at the max SSC.

*We have changed our wording to avoid the word minima, since our primary observation is that depleted DO occurs in locations of elevated SSC—not that the absolute minimum of DO coincides with the absolute maximum of SSC. We make this point clear now by pointing out that the minimum of oxygen is located 3.5 km upstream of the maximum SSC. In fact, the model shows that horizontal advection and diffusion can move the DO minimum on the order of several*

*km from the SSC maximum. So while our primary conclusion holds, i.e., that DO depletion is proportional to SSC, second order affects slightly affect the position of the DO minimum.*

11. Line 181, equation (2), can you provide some reference for this formula, and discuss a little bit about the limitation of this equation?

*We have added a reference to Odd, 1988, and have added the term 'linearized', which implies that the equation is a first order approximation.*

12. Line 184, can you specify what is /rho_s?

*Thanks for the observation--we have now defined this term.*

13. Line 200, equation (5) is given out of the blue, can you provide the derivation or a reference to an article, and describe its limitations? This appears to be a modified gravitational circulation from a conceptual model, rather than from a strict analytic model. But anyway, it should be described properly, or it is hard to assess the suitability and limitations, if any, of the following equations.

*We agree that the introduction of this equation was rather abrupt. We now include several descriptive sentences about the momentum and mass balance equations, and make clear references to supplement S.1 and Talke et al., (2008,2009) which derive these equations.*

**Detailed reply to Reviewer #2:**

I find this to be a very interesting paper, albeit a bit hard to read with all of the sensitivity analyses described in great detail.

*We thank the reviewer for these encouraging comments and have reworked the paper to be easier to read. We have done this by focusing on fewer, but more salient, model results and by improving the figures. The detailed sensitivity studies have been placed into supplementary sections. In these ways the paper should be more accessible for the E&C community.*

I think the paper could be of significant importance, but I would like to have seen at last a few comparisons between the model and observations. They apparently have access to a great deal of observations (see for example, Figures 3-5), but they want the readers to just believe, for example, that their assumptions of salinity (Equation 3) and SSC (Equation 4) physical structure are acceptable. Some data would be more convincing.

*We have added data and analysis to justify our longitudinal salinity equation and vertical SSC equation to supplement S.2 (to put into the main text would distract from the primary purpose of the paper, which is to investigate oxygen depletion). In addition, we reference Warner et al., 2005, who use the same functional form of the longitudinal salinity equation.*

Also, before describing the many sensitivity tests, it would be nice to know if the 1D and 2D model actually reproduce the observed structure and dynamics. They show no comparisons. Even with good comparisons to observations, one always wonders if the internal controls in model are real, but without showing the model matches observations, it is not appropriate to imply that what controls the model, controls the environment.

*We now explicitly compare the 1D model results to data measured at fixed points, and use the experimental data to determine our estimates of the coefficients of aeration, sediment oxygen demand, and suspended organic material decay. This has resulted in a new set of DO model parameters that we feel are more robust. The overall conclusions of the paper have not been altered, however.*

*In the discussion of the estuarine, 2D DO model we now make more explicit comparisons with data and show that the magnitudes and distribution of modeled DO and SSC are similar, qualitatively, to the longitudinal measurements in Fig. 2 and Fig. 3. However, more direct comparisons are not possible because (a) the measured SSC and DO in Fig. 2 and Fig. 3 are snapshots during a tidal period, rather than a tidal average and (b) the idealized model is designed to investigate the underlying physics, rather than be rigorously predictive. Hence, we feel a good qualitative agreement between the estuarine model and measurements is sufficient to validate the model and explore the underlying physics.*

I think the paper would be much more appropriate for this journal if it first demonstrated its ability to reproduce observed dynamics in the Ems. While the last sentence of the abstract makes that claim, they do not provide evidence.

*We have addressed this comment in several ways, both by improving our presentation of historical changes and by more explicitly comparing the model to the measurements.*

*First, we have established more clearly that the DO distribution has changed in the Ems over the past 20 years (Fig. 4 and Fig. 5), and that this change is primarily observed between 0.5 psu and 2 psu, where the SSC maximum resides. We now establish that the changes in DO are probably related to changes in the magnitude of SSC, which makes it possible to compare observed long-term trends in the field data with our SSC and DO model results. Our model produces results that are consistent with the observed changes, and shows that the primary cause of increased SSC and decreased DO was likely the increase in the depth of the shipping channel.*

*Second, we now explicitly compare the modeled and measured variation in DO as a function of both SSC and temperature (section 4.1). Hence, we model two important components of DO variation: seasonal variations to temperature, and longer term variations due to SSC changes.*

# An idealized model and systematic process study of oxygen depletion in highly turbid estuaries

S.A. Talke[1], H.E. de Swart[2], V.N.de Jonge[3]

(1): Civil & Environmental Engineering Department, University of Washington
201 More Hall, Box 352700
Seattle, WA 98195-2700 USA
e-mail: stalke@u.washington.edu

(2): Institute for Marine and Atmospheric research, Utrecht University,
Princetonplein 5, 3584 CC Utrecht, the Netherlands
e-mail: h.e.deswart@uu.nl

(3): Institute of Estuarine Coastal Studies (IECS), University of Hull
Hull, HU6 7RX, United Kingdom
e-mail: v.n.de.jonge@planet.nl

Keywords: Estuarine circulation, Estuarine Turbidity Maximum, Sediment Dynamics, Morphology, Fluid Mud, Water Quality, Hypoxia, Anoxia, Ems Estuary

## ABSTRACT

The sensitivity of oxygen depletion in turbid estuaries to parameters like freshwater discharge, depth and sediment availability is investigated using an idealized model. The model describes tidally-averaged circulation and suspended sediment concentration (SSC), which are input into an advection-diffusion-sink module of dissolved oxygen (DO). Based on the analysis of field data collected in the Ems estuary, the modeled oxygen depletion rates are proportional to SSC. The model is calibrated to the observed variation of DO with SSC and temperature. Modeled DO closely tracks changes to the estuarine turbidity zone (ETZ): increased channel depth, decreased freshwater discharge, and decreased mixing move the ETZ upstream, amplify SSCs and decrease DO. Summertime temperatures produce lower DO than cooler periods. Model results are consistent with historical measurements in the Ems, which indicate that hypoxic events (DO concentrations < 2mg $l^{-1}$) have occurred more frequently after deepening from 5 m to 7 m.

## INTRODUCTION

Depleted levels of dissolved oxygen (DO) occur in many Asian estuaries (Fang & Lin, 2002, Dai et al., 2006, and Ni et al., 2007), North American estuaries (Engle et al., 1999, Borsuk et al., 2001, Hagy et al., 2004, Benoit et al., 2006, and Lin et al., 2006), and European estuaries (Uncles et al., 1998, Garnier et al., 2006). These zones of hypoxia (DO concentration < 2 mg $l^{-1}$) greatly degrade environmental conditions for benthic and pelagic fauna and alter redox conditions, which changes the cycling of nutrients and partitioning of pollutants throughout the estuary (de Jonge & Villerius, 1989, Diaz & Rosenburg, 1995, Nestlerode & Diaz, 1998, Fang & Lin, 2006). Given the ecological consequences of hypoxic and anoxic conditions, there is a strong need to understand, on a process level, the physical and biological processes that are contributing to this problem.

In many estuaries, oxygen depletion is tied to the inputs of organic matter caused by effluent, industry, or natural causes (Hagy et al., 2004, Dai et al., 2006, Fang & Lin, 2006, Wei et al., 2007). Other estuaries such as the Humber Estuary, Loire Estuary, and Yellow River Estuary show evidence of oxygen depletion due to the degradation of organic matter that is associated with the suspended sediment aggregates (Uncles et al., 1998, Thouvenin et al., 1994, Ni et al., 2007). Physical processes which affect DO concentrations include vertical mixing and stratification, river discharge, and baroclinic circulation. In the Chesapeake Bay region, high river inflow causes greater influx of nutrients, greater primary production, and subsequent depletion of DO (Hagy et al., 2004, Lung & Nice, 2007). In other estuaries, hypoxic conditions occur during low inflow conditions and are attributed to the increased residence time of water (Dai et al., 2006, Hagy & Murrell, 2007). Vertical mixing often controls DO,

59 with depletion occurring in highly stratified systems (Borsuk et al., 2001, Lin et al., 2006,
60 Hagy & Murrell, 2007). Finally, an idealized analytical model and a box model show that
61 gravitational circulation, which drives near-bed flows of oxygenated seawater into the estuary,
62 also alters the oxygen budget of estuaries (Lin et al., 2006, Hagy & Murrell, 2007).
63
64 In this paper we investigate oxygen depletion that occurs in the estuarine turbidity zone (ETZ)
65 of the Ems estuary. Before the 1980s, hypoxic conditions occurred primarily in the Dollard
66 sub-basin from the discharge of organic matter (e.g., sewage effluent), particularly when low
67 freshwater discharge resulted in a large residence time of water (Helder & Ruardij, 1982).
68 Though sanitation measures greatly reduced the organic load and oxygen depletion in the
69 Dollard (Essink, 2003), we present measurements which show that low DO concentrations
70 are increasingly being measured in the brackish and freshwater portions of the river Ems,
71 upstream of the Dollard. Using a combination of field measurements and modeling, we
72 investigate the cause of the renewed water quality problem , focusing on the connection
73 between depleted DO and increased suspended sediment concentrations (SSCs) in the
74 turbidity zone. The physical mechanisms behind decreasing DO concentrations and
75 increased turbidity are investigated with an idealized, tidally averaged model that estimates
76 circulation, SSC (organic matter), and DO concentrations. Estuarine geometry, physical, and
77 biological processes are simplified to investigate first order effects, and result in a model of
78 oxygen depletion that is transparent, computationally fast, and flexible. Using sensitivity
79 studies, we identify key parameters that govern observations. For turbid estuaries, we show
80 that the along-channel distribution of organic material—which is set by the sediment
81 dynamics of turbidity zones—governs the depletion of DO.
82

## 2. Observational Background

The Ems-Dollard estuary, located on the border of the Netherlands and Germany, is forced by semidiurnal tides with tidal ranges increasing from 2.3 m at the inlet to ~ 3.5 m in the river (Fig. 1). Approximately 80% of the Dollard sub-basin, and ~50% of the entire estuary, is covered by tidal flats. Channel depth is maintained at a navigable depth of 8 m from the barrier island of Borkum (km 0) to the harbour town of Emden (km 46; Krebs and Weilbeer, 2008), with a maximum depth of ~ 30 m and is maintained at ~ 7 m depth for shipping between Emden and Papenburg (km 87). A tidal weir at Herbrum (km 100) marks the end of tidal influence. Freshwater discharge average varies from 10-40 $m^3s^{-1}$ during the summer months to a maximum of ~ 600 $m^3s^{-1}$ during wet winter periods (yearly average is 80-110 $m^3s^{-1}$). The watershed of the Ems contains large areas of peat, which leads to highly refractory organic material in the estuary (van Es et al., 1980, Baretta & Ruardij, 1988). Water temperature varies from $0^o$-$25^o$ Celsius between winter and summer.

We use a combination of moored, monitoring data and cruise data to analyze oxygen depletion. For the years 2005-2006, salinity, SSC, temperature, freshwater discharge, and DO concentration measurements at 5 - 30 minute increments were made available at 8 stations along the Ems by the Niedersächsisches Landesbetrieb für Wasserwirtschaft, Küsten-und Naturschutz (NLWKN), part of the German state of Niedersachsen (see Fig. 1). We also use historical measurements of salinity, DO, and temperature from the stations at Leer- Leda (located 3.9 km upstream of Ems km 73.3 on the Leda tributary) and Terborg (km 62.7), which are available from 1984-2000 and 1988-2000, respectively, from the NLWKN. Historical measurements of turbidity and SSC are available at Leer-Leda and Terborg, respectively, from 1998-2000.

Beginning in February 2005 and running through December, 2007, 30 (nearly) monthly measurements of water quality and biological parameters were made along the longitudinal axis of the Ems estuary using a ship-board flow-through system (see Fig. 1). On selected cruises we measured vertical profiles of turbidity, salinity, temperature, and dissolved oxygen (DO) concentration using an RBR Conductivity-Temperature-Depth Sensor (CTD) with an attached DO sensor. Profiles of velocity and backscatter were also made with an RDI work-horse ADCP. Water samples from each cruise were filtered using a Whatman GF/C filter to determine the suspended sediment concentrations (SSCs) and calibrate the OBS using the method of Kineke & Sternberg (1992). Here we focus on CTD/DO casts obtained during a cruise between km 45 (near the port of Emden) and km 100 (the tidal weir at Herbrum) on Aug. 2, 2006 during low freshwater discharge conditions (see Fig. 2 and Fig. 3). The outgoing cruise progressed upstream with the ebb tidal wave (against the current), beginning at 4 hours before the local Low Water (LW) slack, and ending at local LW-slack. The return cruise progressed against the flood tide wave (against the current), starting about 2 hours after local LW (~3.5 hrs before HW slack) and ending ~ 30 minutes after local HW slack. Overall, 25 CTD/DO casts were made in 2-3 km increments during the outgoing ebb cruise and 14 casts were made during the return flood cruise. Measurements near each other, particularly at the important transition from turbid to clear conditions and marine to freshwater, are nearly synoptic (see Fig. 2, Fig. 3); more information is available in Talke et al. (2009).

**2.2 Field Results**

Measurements along the longitudinal axis of the Ems estuary from Aug. 2, 2006 show evidence of widespread hypoxia (DO < 2 mg $l^{-1}$) and wide variation in SSCs (0.3-80 kg $m^{-3}$) during both ebb (Fig. 2) and flood (Fig. 3) tides. Water is relatively clear (SSC < 0.5 kg $m^{-3}$) in the more marine portion of the estuary (salinity > 10 psu) but is extremely turbid with large SSCs and fluid mud (10-80 kg $m^{-3}$) in the brackish regions (salinity < 2 psu ). The elevated SSC, which forms an estuarine turbidity zone (ETZ) from the toe of the salt wedge (km 65 to km 75) to the tidal weir (km 100), coincides with a zone of depleted dissolved oxygen (DO) with concentrations less than 5 mg $l^{-1}$ (with a minimum below 1 mg $l^{-1}$). More saline water (salinity > 5 psu) is well oxygenated. Both SSC and DO vary vertically, with SSC increasing exponentially towards the bed (see Supplement S.2) and DO as much as 2 mg $l^{-1}$greater at the surface than near the bed. Salinity over most of the estuary is vertically well mixed or partially mixed. The depleted DO zone persists during both the ebb and the flood, over different phases of the tidal wave. As sediment moves upstream during the flood tide in Fig. 2, the zone of depleted oxygen also moves upstream (compare Fig. 2 and Fig. 3). Other spatial patterns of SSC, such as the local maximum in SSC at km 65 during the ebb, also correspond with reduced oxygen concentration (Fig. 2). The overall minimum DO during the quasi-synoptic ebb cruise is located at km 73.8, about 3.5 km upstream of the maximum SSC of ~ 80 kg $m^{-3}$ (Fig. 2). Water temperatures ranged from 21 $^{o}$C (marine water) to 24 $^{o}$C (at the weir).

The observed relationship between high SSC and depleted oxygen concentrations indicates that organic matter in the fluid mud is controlling the depletion of oxygen in the water column, as also observed in other turbid estuaries such as the Humber (Uncles et al., 1998). Historical measurements at two fixed stations confirm that oxygen depletion correlates well with SSC (Fig. 4 and Fig. 5). Figure 4a and 5a show envelopes of the average DO and its

standard deviation as a function of SSC, with DO measurements separated into water temperature bins reflecting typical summer conditions ($18^o$-$21^o$ C), spring and autumn conditions ($9^o$-$12^o$ C) and winter conditions ($0^o$-$3^o$ C). At both locations, DO concentrations decrease approximately linearly with increasing SSC (Fig. 4a) and turbidity (proportional to SSC; Fig. 5a), although the slope decreases slightly at higher SSC. Dissolved oxygen concentrations are a strong function of temperature: colder water is more oxygenated at zero SSC and the rate of depletion as a function of SSC is smaller. Significant variation (standard deviation of $\sim \pm 1$ mg $l^{-1}$) is found in the trends observed in Fig. 4a and 5a. A partial list of possible causes include changing aeration due to wind, variable mixing due to tides (e.g., spring-neap), advection and diffusion from upstream and downstream, recent conditions (e.g., conditions over the previous time period), changes in biological factors, or other sources of DO depletion (e.g., patchiness in distribution of organic material or micro-organisms). Nonetheless, to first order, the depletion of DO can be considered to be proportional to SSC.

The SSC which causes DO depletion is typically trapped within an estuarine turbidity zone which is centered within a band of salinity between 0.5 psu and 2 psu (Fig. 4c and 5c). At low salinity (< 0.3 psu), which occurs during elevated freshwater discharge at these locations, SSC and turbidity decrease markedly. Conversely, the salt wedge moves upstream during low discharge and the measured SSC decreases as salinity increases (> 2 psu). Because the station of Leer-Leda (Fig. 5) is nearly 15 km upstream of Terborg (Fig. 4), salinity does not exceed 2 psu.

The SSC and turbidity distribution suggests a conceptual picture in which organic material (attached to SSC) produces a sag (minimum) in the along estuary distribution of DO, with more oxygenated conditions observed at the freshwater and saline boundaries of the ETZ (see

182 also Fig. 2 and Fig. 3). Such a DO sag is confirmed by contemporary measurements from
183 1998-2000, which show that DO concentrations increase markedly during freshwater
184 conditions (Fig. 5b) and more marine conditions (Fig. 4b), with minimum DO concentrations
185 occurring in brackish water between 0.5-2 psu. Comparison with historical measurements
186 from 1988-1990 (Fig. 4b) and 1984-1986 (Fig. 5b) show a downwards shift in DO in the ETZ
187 of between 1-3 mg $l^{-1}$, on average. No significant change in DO is observed at the boundaries
188 of the ETZ. Hence, though historical measurements of SSC are unavailable, the results
189 indicate that the increased oxygen depletion in the ETZ is likely occurring because of
190 increased SSC (and not other factors). The majority of increased oxygen demand apparently
191 occurred after 1993, since mean DO concentrations in 1991-1993 are only slightly less than
192 1984-1986 (Fig. 5b). The decrease in DO concentrations (particularly after 1994) coincides
193 with progressive deepening of the river Ems in 1985-1986, 1991-1992, and 1994 from ~ 5 m
194 to ~ 7 m between Emden (km 46) and Papenburg (km 87; Jensen et al., 2003), and increased
195 maintenance dredging (de Jonge, 2000).
196
197 The worsening DO conditions over the past 2 decades are confirmed by considering the time
198 (measured in days per year) that DO concentrations are below the threshold of 5 mg $l^{-1}$ and 2
199 mg $l^{-1}$ (Fig. 4d and Fig. 5d). Whereas less than 20 days per year dipped below the 5 mg $l^{-1}$
200 threshold before 1991 at either station, conditions worsen to a high of ~118 days in 2005 at
201 Terborg (data is unavailable past 2000 for Leer-Leda). Hypoxic conditions (< 2 mg $l^{-1}$) never
202 occurred at either station before 1997, but are becoming increasingly common and are
203 occurring for longer time periods (~ 20 days in 2005). Because DO concentrations of 5
204 mg $l^{-1}$ and 2 mg $l^{-1}$ are thresholds below which many fish and other organisms become stressed
205 or killed, respectively, the environmental quality of the river Ems has clearly degraded.
206

Because the DO sag in the Ems estuary is linked to the magnitude of SSC and its longitudinal distribution, understanding the physical factors which change the ETZ (e.g., freshwater discharge or water depth) becomes essential for understanding DO dynamics. The persistence of elevated SSC and depressed DO during both the flood and ebb (Fig. 2 and Fig. 3) suggests that a tidally averaged model can capture the sub-tidal distribution of SSC and DO. To identify and understand the physical factors controlling oxygen depletion, we next develop an idealized model for the distribution of SSC and DO in an estuary.

## 3. MODEL

The oxygen depletion model we develop for an idealized estuary uses analytical solutions to tidally averaged circulation and SSCs developed by Talke et al. (2008, 2009). Here we first outline the hydrodynamic and morphodynamic models (more details are available in Supplement S.1), and then develop the DO concentration model.

### *3.1 Hydrodynamic and SSC model*

The tidally averaged hydrodynamic model of Talke et al. (2008, 2009) extends the classical definition of estuarine circulation (Hansen and Rattray, 1965, Officer, 1976) to include currents that arise due to longitudinal density gradients of SSC. The model applies the rigid-lid assumption, assumes no-slip at the bottom boundary, no shear at the top, and assumes that eddy viscosity $A_v$, eddy diffusivity $K_v$, depth $H$, longitudinal dispersion $K_h$, and the settling velocity $w_s$ of sediment particles are constant throughout the model domain (see Fig. 6 for a review of key assumptions). The $x$-axis points upstream and the origin $x = 0$ is at the seaward

boundary. The *z*-axis points upwards from the water surface. Following other idealized studies (e.g., Friedrichs et al., 1998), we define a funnel shaped estuary such that the development of width *b* with distance is described by an exponential function,

$$b(x) = B_o \exp\left(\frac{-x}{L_e}\right), \quad (1)$$

where $B_o$ is the width at the estuary mouth ($x$ = 0) and $L_e$ is the convergence length-scale of the estuary. Following Odd (1988), the equation of state for the model is a linearized function of both salinity *s(x)* and suspended sediment concentration *C(x,z)*:

$$\rho(x,z) = \rho_o + \beta s(x) + \gamma C(x,z)\,. \quad (2)$$

In this expression, *ρ(x,z)* is the combined density [kg m$^{-3}$], $\rho_o$[kg m$^{-3}$] is the density of water, *ß* is ~ 0.83 kg m$^{-3}$psu$^{-1}$ and converts salt to density and $\gamma = (\rho_s - \rho_o)/\rho_s \sim 0.62$ converts SSC into density, where $\rho_s$ is the density of the sediment particles, here assumed to be sand for simplicity. We assume that salinity is well mixed vertically (as suggested by Fig. 2 and Fig. 3) and is described longitudinally by a hyperbolic tangent (see also Warner et al., 2005):

$$s(x) = 0.5 S_o \left\{1 - \tanh\left(\frac{x - x_c}{x_L}\right)\right\}, \quad (3)$$

where $S_o$ [psu] is the salinity at the seaward boundary, $x_c$ [m] is the position of the maximum salinity gradient, and $x_L$ [m] scales the slope of the salinity gradient. The parameters $x_c$ and $x_L$ are functions of freshwater discharge, as summarized in Table 1 and described in more detail in Supplement S.1.

The vertical distribution of SSC is modelled as an exponential profile, a consequence of assuming that the settling flux of particles is balanced by an upward flux from turbulent diffusion:

$$C(x,z) = c_b(x)\exp\left\{\frac{-w_s}{K_v}(z+H)\right\}, \quad (4)$$

where $c_b(x)$ is a function describing the distribution of SSC at the bed (located at $z = -H$) in the longitudinal direction. As described in Supplement S.2, SSC measurements at a fixed location in Feb. 2006 show that, to first order, an exponential profile of SSC with depth is a valid approximation over a tidal period. We assume that, to first order, there are no tidally averaged transverse variations in SSC.

The tidally averaged momentum equation describes a balance between the barotropic pressure gradient induced by the time-averaged surface slope and the baroclinic pressure gradient induced by the combined longitudinal variation in SSC and salinity (Eq. 2). Further, the cross-sectionally integrated flow at each point $x$ is set equal to the freshwater discharge $Q$ (which is taken as negative in our coordinate system). Solving these expressions with appropriate boundary conditions, as discussed in more detail in Supplement S.1, yields:

$$u(x,\zeta) = \underbrace{\frac{g\beta H^3}{48\rho_o A_v}k_1(\zeta)\frac{ds}{dx}}_{baroclinic\ circulation} + \underbrace{\frac{g\gamma H^3}{48\rho_o A_v}k_2(\zeta, Pe_v)\frac{dc_b}{dx}}_{SSC\ induced\ circulation} + \underbrace{\frac{3Q}{2b(x)H}(1-\zeta^2)}_{freshwater\ circulation}, \quad (5)$$

where $\zeta = z/H$ is the non-dimensional height, $g$ is gravity, and $Pe_v = w_s H / K_v$ is the vertical Peclet number for SSC. The first term on the rhs of Eq. 5 is baroclinic circulation due to the prescribed salinity gradient $ds/dx$ , the second term is circulation due to gradients in bottom SSC ($dc_b/dx$), and the third term is the contribution of freshwater discharge and is a function

of the width $b(x)$. The vertical structure of flows driven by longitudinal salinity gradients and longitudinal SSC gradients are described by the functions $k_1$ and $k_2$, respectively, and are defined in the appendix. When $dc_b/dx$ is set to zero and $b(x)$ is constant, the gravitational circulation model of Hansen and Rattray (1965) is recovered. Flow is assumed uniform over the width.

The function $c_b(x)$ is found by first assuming that the model estuary is in morphodynamic equilibrium, i.e., that tidally averaged SSC concentrations over time are constant for a given set of parameters (more detail is given in Supplement S.1). Morphodynamic equilibrium occurs when net sediment transport over a transverse cross-section vanishes, and is defined for a variable width, constant depth model as follows:

$$\int_{-H}^{0}\int_{-b/2}^{b/2}\left\{uC - K_h\frac{\partial C}{\partial x}\right\}dydz = 0\,, \tag{6}$$

where the first term in brackets ($uC$) is advective flux and the second term is dispersive flux. The model is closed by defining the total mass of SSC over the entire model domain,

$$c_* HL\langle b\rangle = \int_{-H}^{0}\int_{-b/2}^{b/2}\int_{0}^{L} C(x,z)b(x)dxdydz\,, \tag{7}$$

where $\langle b\rangle$ *is* the average width, $L$ is the length of the model domain, and the user-defined parameter $c_*$ is the average SSC over the model domain. For a given average concentration $c_*$, the morphodynamic equilibrium (Eq. 6) is solved analytically, using Eq. 1, Eq. 4, and Eq. 5, to define the equilibrium distribution of SSC:

$$C(x,z) = A_1 \underbrace{exp(\,F(x)\,)}_{\substack{longitudinal\\component}} \underbrace{exp\left\{\frac{-w_s}{K_v}\,(z+H)\right\}}_{vertical\ component}, \tag{8a}$$

299
300

$$F(x) = \underbrace{\frac{-T_s g\beta H^3 s(x)}{48\rho_o A_v T_K K_h}}_{\substack{baroclinic \\ component}} \underbrace{- \frac{T_T g H^3 c_b(x)}{48\rho_o A_v T_K K_h}}_{SSC\ component} + \underbrace{\frac{3T_Q Q L_e}{2HT_K K_H b(x)}}_{freshwater\ component}, \quad (8b)$$

301

302 where $T_S$, $T_Q$, $T_T$, and $T_K$ are parameters that are defined in the appendix. The longitudinal
303 distribution of salinity, SSC, and freshwater discharge all contribute to the equilibrium
304 distribution of sediment. The definition of $c_*$ is used to find the constant $A_1$:

305

$$A_1 = \frac{c_* Pe_v L < b >}{(1 - exp\{-Pe_v\}) \int_0^L b(x) exp\{F(x)\} dx}. \quad (9)$$

306

307 Equations 8-9 are solved iteratively, as described in Supplement S.1.

308

309 3.2 *Oxygen consumption by suspended sediment oxygen demand*

310

311 In typical rivers and estuaries, the depletion of oxygen occurs from the consumption of
312 organic material and is expressed as biological oxygen demand (BOD), sediment oxygen
313 demand at the consolidated bed (SOD), chemical oxygen demand (COD), and nitrogen
314 oxygen demand (NBOD) (Cox, 2003). BOD occurs on individual molecules, colloidal
315 material, and on detritus associated with suspended sediment aggregates in the water column.
316 Here we focus on oxygen depletion due to sediment-linked biological material that is trapped
317 at the estuarine turbidity maximum. Measurements show that the organic content of SSC in
318 the Ems ranges from 10-20%, and consists of refractory (relatively 'old') material with a slow
319 degradation rate and rate of oxygen consumption (personal communication, A. Scholl; Wurpts
320 & Torn, 2005). However, because near bottom SSCs exceed 50 kg $m^{-3}$ (see Fig. 3 and Fig. 4),

the total organic material and oxygen demand is capable of depleting oxygen. To gain better understanding of the effect of elevated concentrations of organic material on DO concentrations, we explicitly neglect the oxygen depleted by NBOD. Similarly, we neglect oxygen added by algal production and consumed through respiration, since high turbidity severely limits light and algal growth (Colijn, 1982; May et al., 2003). These processes are left for future study.

To model the depletion of oxygen ($O_2$) due to organic material in the water column, we assume that the oxygen consumption within a control volume is proportional to the concentration of organic material, which in turn is proportional to SSC. This rate of change is modified by a factor of $O_2/(k_m + O_2)$, where $k_m$ is a constant which is typically set equal to 0.7 $\times 10^{-3}$ kg m$^{-3}$ (Cox, 2003). This factor ensures that the rate of oxygen consumption goes to zero in the limit of zero oxygen concentration. Hence, we define the suspended sediment oxygen demand (SSOD) to be

$$SSOD = \frac{-O_2}{k_m + O_2} p k_r(T) C(x,z), \tag{10}$$

where $p$ is the percent organic material in the SSC and is set to 0.1, and $k_r$ [s$^{-1}$] is a (positive) rate of decay of organic (carbonaceous) material that varies with temperature $T$. The temperature dependence is based on the Arrhenius relation, and is commonly modelled as $k_r(T) = k_{ref}\theta^{1/T_o(T-T_{ref})}$, where $\theta$ is a parameter which ranges from 1.04 to 1.13, $T_{ref}$ is a reference temperature of 20$^o$ C, and $T_o$ =1$^o$ C is a dummy variable applied to retain non-dimensionality (see Cox, 2003). Reported values for the organic material decay coefficient (carbonaceous oxygen demand) at 20 degrees Celsius, $k_{ref}$, ranges from ~$10^{-7}$ s$^{-1}$ to $2.3 \cdot 10^{-5}$ s$^{-1}$, or 0.01 day$^{-1}$ to 2.0 day$^{-1}$ (Williams, 1993; Cox, 2003). We use a value of $k_{ref}$ that is an order

of magnitude smaller ($1.3\ 10^{-8}\ s^{-1}$), as described in section 4.1 (see Table 2). To maintain consistency in the units, we express oxygen $O_2$ in units of kg $m^{-3}$ in the model; in the results section, we convert $O_2$ to the more commonly reported units of mg $l^{-1}$.

Next we apply the control-volume approach to oxygen fluxes in the model estuary, applying the assumption that horizontal velocity $u$, vertical velocity $w$, $O_2$, longitudinal dispersion $K_h$, and eddy diffusivity $K_v$ are uniform over the width. The kinematic conditions for velocity are applied at the side-walls ($y = +/- b/2$), and no normal flux of oxygen is assumed through these boundaries. Assuming steady conditions and integrating over width, the mass balance of $O_2$ becomes

.

$$0 = \frac{\partial}{\partial x}(buO_2) - \frac{\partial}{\partial z}(bwO_2) + \frac{\partial}{\partial x}\left(bK_h\frac{\partial O_2}{\partial x}\right) + \frac{\partial}{\partial z}\left(bK_v\frac{\partial O_2}{\partial z}\right) - b\frac{O_2}{k_m + O_2}pk_rC\,. \qquad (11)$$

The first two terms on the right hand side are the convergence of width-integrated advective flux of DO, the third and fourth terms are the convergence of width-integrated diffusive flux of DO, and the last term is the sink of DO. We simplify using the continuity equation (mass balance of water),

$$0 = \frac{\partial}{\partial x}(bu) + \frac{\partial}{\partial z}(bw), \qquad (12)$$

which yields the following equation for $O_2(x,z)$,

$$0 = \underbrace{-u\frac{\partial O_2}{\partial x} - w\frac{\partial O_2}{\partial z}}_{\text{advection}} \underbrace{-\frac{K_h}{L_e}\frac{\partial O_2}{\partial x} + K_v\frac{\partial^2 O_2}{\partial z^2} + K_h\frac{\partial^2 O_2}{\partial x^2}}_{\text{diffusion}} \underbrace{-\frac{O_2}{k_m + O_2}pk_rC}_{\text{sink}}\,. \qquad (13)$$

The vertical velocity, *w*, is found from continuity (Eq. 12), using Eq. 1 and the solution from Eq. 5. The term $-\frac{K_h}{L_e}\frac{\partial O_2}{\partial x}$ arises from the transport caused by the width convergence of the estuary; for channels ($L_e$ large), this term becomes negligible. Because sediment concentration *C(x,z)* and the velocity *u*(*x,z*) are known analytically by Eq. 8 and Eq. 5, respectively, only DO concentrations are unknown and must be solved for using the appropriate boundary conditions. At the consolidated bed, we assume that oxygen is consumed by the sediment oxygen demand, SOD, at the rate $S_b(T)$, [kg $O_2$ $m^{-2}$ $s^{-1}$],

$$K_v \frac{\partial O_2}{\partial z}\bigg|_{z=-H} = \frac{O_2}{k_m + O_2} S_b(T)\bigg|_{z=-H}. \quad (14)$$

In analogy with oxygen demand in the water column (Eq. 10), we model the effect of temperature as $S_b(T) = S_{br}\theta^{1/T_o(T-T_{ref})}$, where $S_{br}$ is a constant at the reference temperature of 20° C, and add the corrective factor $O_2/(k_m + O_2)$ to ensure that negative DO concentrations cannot occur. Typical river and estuary values of $S_{br}$ range from ~$10^{-9}$ kg $O_2$ $m^{-2}$ $s^{-1}$ (sandy or mineral bed) to $10^{-7}$ kg $O_2$ $m^{-2}$ $s^{-1}$ (organic deposits), with typical estuarine values of ~ 1-2·$10^{-8}$ kg $O_2$ $m^{-2}$ $s^{-1}$ (Chapra, 1997). In the muddy Seine estuary, measurements by Garban et al., 1995 reported an SOD value of 3.2· $10^{-8}$ kg $O_2$ $m^{-2}$ $s^{-1}$, with a range of 1.7· $10^{-8}$ kg $O_2$ $m^{-2}$ $s^{-1}$ to 8.3 · $10^{-8}$ kg $O_2$ $m^{-2}$ $s^{-1}$. We calibrate our model using these reported ranges of SOD in section 4.1. At the surface, the flux of oxygen between the atmosphere and the water column is proportional to the difference between saturated conditions ($O_{2,sat}$) and actual conditions ($O_2|_{z=0}$):

$$K_v \frac{\partial O_2}{\partial z}\bigg|_{z=0} = k_L\left(O_{2,sat} - O_2|_{z=0}\right), \quad (15)$$

where $k_L$ [m $s^{-1}$] is an empirical constant that depends on climatic conditions, depth, and hydrodynamic conditions (see e.g. Cox, 2003). The flux of oxygen at the surface is often assumed to be a constant on the order of $10^{-8}$ kg $O_2$ $m^{-2}$ $s^{-1}$ (Lin et al., 2006). Here, we allow the flux $k_L\left(O_{2,sat} - O_2|_{z=0}\right)$ to vary based on the oxygen deficit at the surface. In the Seine River, Garnier et al. (2001) found values of the aeration coefficient $k_L$ along different reaches to be between 0-0.07 m $hr^{-1}$, with averages between 0.02-0.07 m $hr^{-1}$ ($5 \cdot 10^{-6}$ m $s^{-1}$ to $2 \cdot 10^{-5}$ m $s^{-1}$). Cox (2003) lists multiple studies with depth averaged values of the aeration coefficient that vary between 0-250 $day^{-1}$ with an order of magnitude of ~ 0.4 $day^{-1}$ for large rivers, or, when scaled by a depth of $H$ = 7 m, approximately $3 \cdot 10^{-5}$ m $s^{-1}$. The saturated oxygen concentration is a function of temperature and salinity and is ~ 8.5 mg $l^{-1}$at 20 $^{o}$C (APHA, 1992). The downstream and upstream boundary condition ($x$ = 0 and $x$ = $L$) is found from the modelled SSC at the boundary, using the simplified 1D-DO model described below. The 2D model is solved using an implicit finite difference algorithm with 100 along-channel grid points and 30 vertical grid points.

To gain fundamental understanding of DO depletion and to obtain an upstream and downstream boundary condition, we simplify Eq. 13 by assuming that horizontal advection and dispersion terms are negligible, to first order (i.e., terms 1, 3, and 5 can be neglected). When applied as a boundary condition, the appropriateness of this assumption must be checked against results. Also assuming negligible vertical velocities, the simplified 1D model requires that

$$0 = K_v \frac{d^2 O_2}{dz^2} - \frac{O_2}{k_m + O_2} p k_r C(z). \qquad (16)$$

412

413 This equation is solved numerically using the boundary conditions described in Eq. 14 and
414 Eq. 15. The vertical variation of SSC, *C(z)*, is prescribed by the parameter $c_*$ (Eq. 7), which
415 in this case reduces to the depth-averaged SSC. For clarity, we denote this depth-averaged
416 SSC by $c_{*d}$, and reserve $c_*$ for the estuary-averaged SSC.

417

418 Equation 16 is further simplified by assuming that the term $\frac{O_2}{k_m + O_2} \sim 1$, which is for
419 approximately valid for DO concentrations above 2 - 3 $\times 10^{-3}$ kg m$^{-3}$ (2 - 3 mg l$^{-1}$). Applying
420 boundary conditions, we find the following analytical solution:

$$O_2 = O_{2,sat} - S_b\left(\frac{-z}{K_v} + \frac{1}{k_L}\right) + \frac{pk_r c_{*d} H/w_s}{\left(1 - exp(-Pe_v)\right)}\left\{\left(\frac{w_s}{k_L} - 1\right) exp(-Pe_v) + exp\left(\frac{-w_s}{K_v}(z+H)\right) + \frac{w_s}{K_v} z - \frac{w_s}{k_L}\right\} \quad (17)$$

421

422 To explore this expression we simplify it by noting that for the typical values of depth *H*,
423 settling velocity $w_s$, and eddy diffusivity $K_v$ in an estuary, the sediment Peclet number
424 $Pe_v = w_s H/K_v$ is much larger than one; physically, this simply means that most SSC is
425 concentrated near the bed, rather than distributed through the water column. Using the
426 resulting simplification that exp(-$Pe_v$)~ 0, we find that oxygen concentration at the surface
427 ($z$=0) and at the bed ($z$ = -$H$) can be approximated as

428

$$O_2(z=0) \approx O_{2,sat} - \frac{S_b + pk_r c_{*d} H}{k_L}, \quad (18)$$

$$O_2(z=-H) \approx O_{2,sat} - \frac{S_b}{k_L}\left(\frac{Hk_L}{K_v} + 1\right) - \frac{pk_r c_{*d} H}{k_L}\left\{\frac{-k_L}{w_s} + \frac{Hk_L}{K_v} + 1\right\}. \quad (19)$$

429

These functions suggest that, for DO above above 2 - 3 $\times 10^{-3}$ kg $m^{-3}$ (2 - 3 mg $l^{-1}$), oxygen depletion near the surface is a linear function of the organic matter (carbonaceous) decay parameter $k_r$, the average concentration of SSC in the vertical ($c_{*d}$), the depth $H$, and the sediment oxygen demand $S_b$, and is inversely proportional to aeration. Near the bed, additional parameters such as eddy viscosity and settling velocity contribute to DO concentrations in the non-dimensional terms $\frac{Hk_L}{K_v}$ and $\frac{-k_L}{w_s}$, and account for water column variation.

## 4. MODEL RESULTS

The model presented in section 3 depends both on vertical water column processes (mixing, aeration, etc) and on the longitudinal structure of SSC and circulation. We first calibrate and validate the model by comparing point measurements of SSC and DO using the vertical water column model described in Eq. 16 (Section 4.1), then address the effect of circulation on the distribution of SSC and DO concentration (Section 4.2).

### 4.1 *Model calibration and validation*

We test and calibrate our DO model by comparing model results (using the simplified, 1D vertical depletion model, Eq. 16) with the measured dependence of DO on SSC at three fixed stations in 2005 and 2006 (Fig. 7). These upstream stations, located between km 72.6 and km 86.9, are within the summertime turbidity zone measured in Fig. 2 and Fig. 3 and record the largest SSCs within the estuary (greater than 25 kg $m^{-3}$ and 50 kg $m^{-3}$, the measurement limits). The large SSC measurement range allows for comparison with the model over a large range of DO. To compare with measurements, the modelled SSC (which uses the vertically

averaged SSC, $c_{*d}$, as an input) is converted to an equivalent point measurement at the sensor depths using the default values of settling velocity, eddy diffusivity, and water depth (see Eq. 4 and Table 2). The sensor depths are located ~2 m, 1.5 m, and 1.5 m above the bed for Fig. 7a to Fig. 7c, respectively. To obtain appropriate model parameters, we next vary the aeration parameter $k_L$ and the bottom sediment oxygen demand $S_b$ within the range reported in the literature (see Eq. 14 and Eq. 15). The carbonaceous decay parameter $k_r$ (see Eq. 10), which is less well established for estuarine conditions, is allowed to float. Physical parameters such as eddy diffusivity and settling velocity are held fixed to remain consistent with the assumptions of the estuarine model. To reduce the effect of temperature, only DO concentrations measured within a small band between 18 $^{o}$C and 21 $^{o}$C are considered (the model temperature is 20 $^{o}$C). The envelope around the mean measured DO indicates the standard deviation.

Two parameter fits of the 1D model are shown in Fig. 7 (see Table 2 for parameter values) and are labeled 'local fit' and 'estuary fit'. Measurements and both fits show initially steep declines with SSC which level out as DO approaches hypoxic conditions (DO < 2 mg $l^{-1}$). Over much of the measured range, both model estimates are within the average standard deviation of 1 mg $l^{-1}$ for the measurement, and the overall root mean square (rms) difference is 0.5 mg $l^{-1}$ for the 'local fit' and 0.8 mg $l^{-1}$ for the 'estuary fit'. Hence, to first order, both fits model the observed variation of DO with SSC. Some divergence between measurements and the 'estuary fit' occurs at zero SSC ($y$-intercept in Fig. 7), with the 'estuary fit' over-predicting the measured DO by 1-2 mg $l^{-1}$ in Fig. 7b and Fig. 7c. Compared to the 'local fit', however, the 'estuary fit' better represents the summertime DO data at zero SSC for Fig. 4a, Fig. 5a, and Fig. 7a, which are ~5.5 mg $l^{-1}$,~7.5 mg $l^{-1}$, and ~5.5 mg $l^{-1}$, respectively. Thus,

479 the ‘estuary fit’ better represents the average oxygen demanded (by SOD) over the estuary
480 when SSCs are small.
481
482 The sediment oxygen demand and aeration in the ‘estuary fit’, $S_b = 3.0\ 10^{-8}$ kg $O_2$ $m^{-2}$ $s^{-1}$ and
483 $k_L = 10^{-5}$ m $s^{-1}$, closely echo values from the muddy Seine estuary measured by Garban et al.
484 (1995) (mean $S_b = 3.2 \cdot 10^{-8}$ kg $O_2$ $m^{-2}$ $s^{-1}$ ) and Garnier et al. (2001) ($5 \cdot 10^{-6}$ m $s^{-1} < k_L <$
485 $2 \cdot 10^{-5}$ m $s^{-1}$ ). Both estimates of the organic material decay rate are an order of magnitude
486 smaller than reported values of carbonaceous decay ($10^{-7}$ $s^{-1}$ Williams, 1993; Cox, 2003), and
487 confirm that the organic material attached to SSC is extremely refractory (see also van Es et
488 al., 1980, Baretta & Ruardij, 1988).
489
490 The simplified, analytical solutions of DO (Eq. 18 and Eq. 19) help explain differences
491 between the measurement sites and models. During clear conditions (zero SSC), the oxygen
492 depletion is set by a balance between sediment oxygen demand (SOD) and aeration, i.e., $S_b/k_L$
493 (see Eq. 18). Hence, the measurement sites in Fig. 7b and Fig. 7c may have less aeration, or
494 greater SOD, than the site in Fig. 7a. Similarly, the slope of DO versus SSC is set by the
495 ratio of organic material decay to aeration, i.e., $k_r/k_L$ (see Eq. 18). Hence the sites in Fig. 7b
496 and Fig. 7c, which have slightly less slopes of DO vs SSC than Fig. 7a, may be exposed to
497 more refractory material (higher $k_r$) or reduced aeration. By contrast, the DO depletion slope
498 in Terborg, km 62.7, is greater than those shown in Fig. 7 (see Fig. 4a), and suggests reduced
499 aeration or higher degradation rates of organic material. These considerations show that the
500 assumption of constant conditions may oversimplify the estuarine model. However,
501 bathymetry, tidal mixing and transport, lateral circulation, and other factors may also affect
502 the measured DO and SSC concentrations, and it is beyond the scope of this contribution to
503 fully consider these factors. Nonetheless, the fit of the model to measurement data (Fig. 7)

504 confirms that that the constant parameter values reasonably model the bulk oxygen depletion
505 occurring due to SOD and SSC over a large portion of the turbid zone.
506
507 The skill of the model in predicting oxygen depletion as a function of temperature is presented
508 in Fig. 8 for both low SSCs (0 - 1 kg $m^{-3}$) and elevated SSCs (18 - 25 kg $m^{-3}$) at three
509 locations (Papenburg, km 86.9; Weener, km 80.1; and Leerort, km 72.6). The measured DO
510 at both low and high SSC is binned into 2 $^{o}$C intervals, and the average is compared against
511 modeled results. The 'local fit' to the ETZ is used for the model (see Table 2), and the
512 average SSC over the water column, $c_{*d}$, is adjusted to produce an SSC of 20 kg $m^{-3}$ at the
513 measurement heights. We find that the parameter $\theta$, used to adjust the DO depletion rates $k_r$
514 and $S_b$ as a function of temperature (see Eq. 10 and Eq. 14), best reproduces measured results
515 with a value of $\theta \sim 1.1$.
516
517 Overall, the measured and modelled variation of DO with temperature agrees to within an
518 rms difference of ~1 mg $l^{-1}$, with both depicting a nearly linear increase in DO as water
519 becomes colder (Fig. 8). Moreover, the model results move closer to saturated conditions as
520 temperature falls and oxygen demand decreases, reflecting the same observation in the
521 measured data. Elevated SSC conditions, labeled 'high SSC', are typically ~1-3 mg $l^{-1}$ less
522 than low SSC conditions in both model and measurements, though some scatter occurs in the
523 data. During warmer (summertime) conditions, DO concentrations approach zero and the
524 observed variation with temperature asymptotes in both the modelled and measured results.
525 Model and measurements of high SSC do not agree well below $T$ = 19 $^{o}$C in Papenburg
526 (Fig. 8a), perhaps because of a paucity of high SSC data at lower temperatures. In Leerort
527 (Fig. 8c), modelled DO slightly overpredicts measurements for low SSC conditions. Besides
528 the processes discussed for Fig. 7, other sources of variation between the model and

529 measurements include variations in decay rates not capture by $\theta$, and the super-saturated DO
530 conditions that are observed to occur periodically at low SSC. Overall, however, the bulk
531 characteristics of the measured and modelled temperature variation agree, and further validate
532 the DO model.
533
534 **4.2 Estuarine model**
535
536 Next, we analyze the patterns of circulation, SSC, and DO concentrations that result in a
537 model 2D estuary from changing freshwater discharge, depth, and mixing. Unless otherwise
538 stated, all parameters are held to the 'estuary fit' parameters displayed in Table 2 and Table 3
539 (SSC model parameters). The hydrodynamic variables in Table 3 represent low freshwater-
540 discharge conditions that occur during the summer months in the Ems estuary (see Talke et
541 al., 2009 for discussion). Parameter studies of settling velocity, horizontal dispersion, width
542 variation, total sediment supply, and longitudinal salinity structure are described in
543 Supplement S.3.
544
545 Figure 9 shows examples of circulation, SSC, and DO concentrations that occur when
546 standard parameters are used (Fig. 9b, Fig. 9d, and Fig. 9f) and when one parameter, depth, is
547 reduced from $H$ = 7 m to $H$ = 5 m (Fig. 9a, Fig. 9c, and Fig. 9e). The model estimates for
548 SSC and DO in the $H$ = 7 m case (standard parameters) qualitatively reproduce the field
549 conditions observed in Fig. 2 and Fig. 3. In both model and measurements, near bed SSCs
550 with magnitudes greater than 10 kg $m^{-3}$ cover the bottom to depths of 1-2 m from the salt
551 wedge to the tidal weir at km 100, and produce a zone of depleted DO that coincides with
552 elevated SSC. The maximum SSC in each occurs between km 70 - 80 (Fig. 2, Fig. 3, Fig. 9).
553 Compared to experimental results (Fig. 2 and Fig. 3), the length-scale of the modelled turbid

554 zone (Fig. 9) is larger, the DO minimum is ~ 0.8 mg $l^{-1}$ greater (perhaps because model
555 temperature is less), and the top-bottom differences in DO concentrations are less.
556 Nonetheless, the overall agreement of the macroscopic (zero$^{th}$ order) trends confirms that we
557 can use our idealized model to investigate the underlying physical processes and resulting DO
558 concentrations.
559
560 A strongly non-linear response in DO and SSC is observed as $H$ is altered from 5 m to 7 m;
561 near bed circulation increases from a maximum of ~ 0.01 m $s^{-1}$ to ~ 0.03 m $s^{-1}$, the maximum
562 SSC is amplified from ~ 9 kg $m^{-3}$ to ~ 60 kg $m^{-3}$, and the DO concentrations are reduced to
563 nearly hypoxic (just over 2 mg $l^{-1}$). The observed changes are driven by the non-linear
564 amplification of baroclinic circulation, which is proportional to $H^3$ and thus increases by a
565 factor of 2.5 (see Eq. 5). By contrast, the magnitude of circulation caused by freshwater
566 discharge is reduced between 5 m and 7 m, since the same inflow $Q$ of -10 $m^3s^{-1}$ is distributed
567 over a greater cross-sectional area. Hence, the downstream penetration of the -0.05 m $s^{-1}$
568 velocity contour from the upstream boundary is greatly reduced for $H$ = 7 m.
569
570 The enhanced near-bed baroclinic flow, coupled with the reduced influence of freshwater
571 discharge, alters the balance of sediment fluxes implied by the condition of morphodynamic
572 equilibrium (Eq. 6). Sediment flux in the upstream direction increases by 2.5 (due to
573 baroclinic circulation), while sediment flux downstream decreases by 5/7 (freshwater
574 discharge). Moreover, for greater depths, sediment is distributed lower in the water column
575 (sediment Peclet number, $Pe_v$, is increased), resulting in more upstream transport. Together,
576 these factors move the turbidity maximum upstream by ~ 10 km as depth is changed from 5 m
577 to 7 m. Because the width of the model decays exponentially upstream ($e$-folding scale of
578 $20 \cdot 10^3$ m), sediment is distributed over a smaller volume of water for $H$ = 7m. As the ETZ

579 moves upstream its longitudinal spread is increasingly halted by the upstream boundary.
580 Finally, the spread of SSC around the maximum is reduced as *H* increases (see Talke et al,
581 2008). Combined, these effects amplify the magnitude of SSC by an order of magnitude, and
582 cause longitudinal gradients in SSC that produce turbidity currents.
583
584 The greatly amplified SSCs for a depth of $H$ = 7 m implies an order of magnitude greater
585 concentration of organic matter. This organic material is primarily responsible for the greatly
586 decreased DO concentrations compared to $H$ = 5 m. Particularly near the bed, deeper water
587 also reduces the affect of aeration and leads to greater DO depletion, due to an increase in the
588 ratios $\frac{pk_r c_{*d} H}{k_L}$ and $\frac{Hk_L}{K_v}$, (see Eq. 19, Supplement S.3).
589
590 For the model estuary, the minimum in oxygen concentration closely follows the position of
591 the maximum SSC, and is 0.4 km and 1.5 km upstream for $H$ = 5 m and $H$ = 7 m,
592 respectively. Moreover, the modelled spread of the low DO area (< 5 mg $l^{-1}$) coincides with
593 the spread of the turbid zone. Hence, for these parameter values, the distribution of sediment
594 is the dominant predictor of DO and longitudinal advection and diffusion of oxygen are lower
595 order effects.
596
597 Variation in freshwater discharge (seasonally) and mixing (e.g., due to spring-neap tidal
598 cycle) are ubiquitous features of an estuary. Fig. 10 presents the modelled effect of
599 increasing freshwater discharge (Figs. 10a,10c,and 10e), or decreasing eddy viscosity and
600 eddy diffusivity (Figs. 10b, 10d, and 10f) from standard conditions (Fig. 9b, 9d and 9f).
601 Increased freshwater discharge directly increases the downstream flow, particularly near the
602 tidal weir where the width $b$ is small. In addition, the salinity field moves and its gradient
603 becomes steeper, leading to a greater baroclinic circulation cell that is shifted downstream by

~ 17 km (Table 1; Supplement S.2). These circulation changes move the ETZ downstream, decrease the longitudinal spread of SSC, and decrease the magnitude of SSC (due to larger width $b$). Increased DO concentrations result, with a smaller DO sag (in the longitudinal direction) shifted downstream with the ETZ.

Reducing eddy viscosity ($A_v$) increases baroclinic circulation (see Eq. 5), while decreasing eddy diffusivity ($K_v = A_v$) causes sediment to accumulate closer to the bed (Fig. 10). Together, the resulting increase in near bed sediment flux (term $uC$ in Eq. 6) moves suspended sediment closer to the boundary, where smaller width and reduced longitudinal spread (due to the upstream boundary) amplify SSCs. These patterns result in greater DO depletion, and an upstream movement in the DO minimum.

A final sensitivity study (Fig. 11) shows changes to the longitudinal distribution of bottom DO ($z = -H$) as parameters associated only with the oxygen model (i.e., $S_b$, $k_L$, $k_r$, and $T$) are varied. In each case, the tidally averaged circulation and equilibrium distribution of SSC resulting from Table 3 default conditions and displayed in Fig. 9b and Fig. 9d, respectively are used. For $S_b$, $k_L$, and $T$, the range of values in Fig. 11 reflects the reported range of each parameter (see section 3.2). For the refractory decay coefficient of organic material, $k_r$, we test the response of a factor of ~2.5 change in either direction.

Increasing bed demand $S_b$ (Fig. 11a), organic material decay coefficient $k_r$ (Fig. 11b), and temperature $T$ (Fig. 11d) result in increased oxygen depletion throughout the model estuary, while increasing aeration $k_L$ (Fig. 11c) produces more oxygenated conditions (note that increasing $T$ raises $S_b$ and $k_r$ simultaneously). The position of the DO minimum changes by several km between different cases, indicating the non-negligible—but 2$^{nd}$ order—affect of

advection and horizontal diffusion. An approximately linear response to changing conditions is observed for aeration above 2 - 3 mg $l^{-1}$, as suggested by the simplified analytical expression (Eq. 18 & Eq. 19): tripling the standard aeration coefficient results in a threefold increase in DO. Decreasing bed demand $S_b$ by an order of magnitude to 10-7 kg $O_2$ $m^{-2}$ $s^{-1}$ approximately doubles the DO concentration (Fig 11a). The less than proportional response occurs because organic material in the water column (given by $k_r$) continues to deplete oxygen. A similar behaviour is observed for decreasing $k_r$ (Fig. 11b).

However, the longitudinal extent of stressed (< 5 mg $l^{-1}$) and hypoxic DO conditions responds non-linearly to changes in the parameters. For example, halving the aeration coefficient from the standard condition produces hypoxic conditions over ~25 km, while tripling aeration removed the stressed area completely (Fig. 11c). Increasing temperature decreases the saturation DO concentration and magnifies both $S_b$ and $k_r$; hence a doubling of temperature from 12 $^{o}$C to 25 $^{o}$C shifts the system from well oxygenated to hypoxic. Changes to water temperature $T$ mirror seasonal changes observed in the river Ems (as low as 0 - 1 $^{o}$C in winter, and 20 - 25 $^{o}$C in summer), and explains why hypoxia occurs primarily in the summer months.

## 5 Discussion

The model we present differs from other models of oxygen depletion in that we consider the depletion of oxygen from a spatially variable SSC. Other models, for example Lin et al. (2006), investigate how gravitational circulation and river discharge affect estuarine residence time and stratification, and therefore the vertical profile of oxygen. In these environments, the mechanism of oxygen depletion is the decay of algae (and thus eutrophication driven) and a

653 constant sediment oxygen demand. Hence, the interaction of nutrients and algae, and their
654 residence time, controls oxygen depletion.
655
656 In highly turbid estuaries, such as the Ems, enormous amounts of SSC are trapped in the ETZ
657 (Figs. 2 - 5). In this situation, a dominant control on the depletion of oxygen becomes the
658 magnitude and distribution of organic matter that is attached to SSCs. This oxygen demand
659 from organic material is neither confined to the bed (as a boundary condition) nor spatially
660 constant over the estuary. A minimum of DO occurs near the turbidity maximum, which is
661 formed when the vertically integrated fluxes of sediment from gravitational circulation and
662 freshwater discharge balance each other. The convergence of these sediment fluxes is
663 balanced by counter-gradient fluxes caused by turbidity currents and longitudinal dispersion
664 (i.e., fluxes proportional to $dc_b/dx$; see Eq. 5 and Eq. 6). Changes to the physical parameters
665 that control these fluxes (e.g., salinity field, freshwater discharge, sediment supply, depth,
666 mixing, etc.) produce a new distribution of SSC and a different spatial variation in oxygen
667 demand and DO. Hence, the factors which alter SSC distribution drive changes to DO, rather
668 than the input of nutrients or the residence time of water.
669
670 Qualitatively, the model results explain the plummet in DO concentrations since deepening
671 the Ems estuary from 5 m to 7 m between 1985 and 1994. The $H^3$ dependence of gravitational
672 circulation produces an inherently non-linear response in SSC transport, which is amplified
673 further by the depth dependence of the area-averaged freshwater discharge and the vertical
674 distribution of SSC. Together, these physical processes cause an order of magnitude increase
675 in SSC and produce a large zone of depleted DO for an increase from 5 m to 7 m (Fig. 9).
676 Additional factors driving DO downwards include the likely decrease in eddy diffusivity and
677 eddy viscosity that occurs due to sediment induced stratification (e.g., Munk and Anderson,

1948). Other variations in mixing –such as the spring-neap cycle—likely drive changes to the ETZ and low DO zone.

Seasonal variation in estuarine DO is driven both by hydrology and water temperature. Depleted DO concentrations occur during the summer months because of low freshwater discharge (which moves the turbidity maximum upstream and amplifies SSC) and elevated temperature (which lowers DO saturation and increases decay rates of suspended organic matter and SOD). By contrast, greater discharge—which occurs during storm events in the winter— decreases SSC and organic matter concentrations by moving the ETZ downstream (van Beusekom & de Jonge 1998; Fig. 10). These conditions combine together with lower temperatures to produce an oxygenated water column in winter.

In ecological terms, the impact of a hypoxic zone is measured by the area of a water body that dips below a biologically critical threshold such as 5 mg $l^{-1}$ or 2 mg $l^{-1}$. Since the modelled oxygen depletion depends on SSC distribution, this equivalently reduces to the length-scale for which SSC is above a certain threshold. The idealized model suggest that the length-scale depends upon the total amount of sediment available for resuspension, the position of the turbidity maximum, and the relative spread of SSC from the maximum (see also Supplement S.3). Changes to organic decay rates, reaeration, and temperature also affect the size of a depleted oxygen zone, and combine together with the SSC distribution to make the system sensitive to relatively small changes in its parameters.

The idealized model we present for the depletion of oxygen makes simplifying assumptions about both physical and biological processes in order to understand, at a process level, the important factors that affect DO depletion from suspended organic matter. The tidally

703 averaged model of circulation and SSC distribution neglects tidally varying processes (e.g.,
704 settling lag, periodic salinity stratification, etc) that influence circulation and the fluxes of
705 sediment in an estuary. Our assumption of constant eddy diffusivity possibly overestimates
706 vertical mixing of DO, particularly in the fluid mud layer, though field results suggest that
707 top-bottom variation is small and generally less than 2 mg $l^{-1}$. Depth and bathymetry effects
708 are likely important, particularly in the less uniform outer estuary. In the oxygen mass
709 balance, we make the further simplifying assumption that model parameters such as the
710 aeration coefficient, the organic matter decay coefficient, and the sediment oxygen demand
711 are constant. In a real estuary, input of organic matter from the rivers and ocean likely cause
712 variation in the decay coefficient, as do phytoplankton detritus, zooplankton detritus, remains
713 of vascular plants, peat, and other sources of carbon. Measurements in the Ems show that
714 organic material is ~ 10% of the SSC for most of the turbid zone, except near the weir where
715 organic material is ~ 20% of SSC and has a larger rate of decay (A. Scholl, personal
716 communication). Greater concentrations of less refractory material near the weir may explain
717 the divergence between modelled and measured results near the weir (compare Fig. 2 and
718 Fig. 9).
719
720 The model assumes that concentrations of algae and other input material are small compared
721 to the mass of organic material trapped at the turbidity maximum, and contribute negligibly to
722 oxygen demand. Given the light limitation in highly turbid waters, phytoplankton production
723 is significant only when SSC is low and is thus away from our zone of interest (e.g., the outer
724 estuary). Similarly, aeration caused by primary production is neglected since the available
725 algae contribute primarily to respiration. For simplicity, the effect of the reduction and
726 oxidation of chemical compounds (e.g., Fe, Mn, and nutrient compounds) and neutrally
727 buoyant colloidal matter on oxygen depletion are also not considered. A complete model of

728 oxygen depletion must include these additional terms and vary them in time and space;
729 however, we explicitly restrict the parameter complexity in order to gain insight into the
730 fundamental effect of sediment dynamics on DO. The overall good qualitative agreement
731 between measurements and the model validates this approach.
732
733
734 **6. Conclusions**
735
736 Measurements in the Ems estuary show that near-bed SSCs exceeding 50 kg $m^{-3}$ coincide
737 with stressed (< 5 mg $l^{-1}$) and hypoxic (< 2 mg $l^{-1}$) DO concentrations. To a first order
738 approximation, the oxygen depletion is proportional to SSC, with the depletion rate
739 decreasing as temperature falls or as anoxic conditions are approached. The zone of depleted
740 oxygen occurs in the estuarine turbidity zone (salinity range of 0.5- 2 psu), which moves as
741 freshwater discharge changes. Over the past two decades, the duration of stressed conditions
742 during summer has increased from 10-20 days to more than 100 days, likely from increased
743 SSCs.
744
745 The physical and biological processes that contribute to oxygen depletion in turbid estuaries
746 are investigated with an idealized model that simplifies estuarine geometry and bathymetry
747 and uses tidally averaged governing equations to investigate first order effects. The depletion
748 rate of DO is assumed to be proportional to SSC, and model calibration to the data shows that
749 the decay rate is extremely refractory. Aeration at the surface provides a source of oxygen,
750 while a prescribed oxygen demand at the bed depletes oxygen. Within the model domain, DO
751 is found by numerically solving an advection-diffusion equation with a sink term, with
752 analytical solutions used for velocity and SSC inputs. At the upstream and downstream

753 model boundaries, DO is approximated by using a 1D vertical water column model which
754 assumes that horizontal flux terms are negligible.
755
756 The modelled depletion of oxygen in the water column is primarily a balance between
757 aeration and the oxygen demand from both the bed (SOD) and suspended sediment.
758 Horizontal advection and diffusion are second order effects that modify, but do not control,
759 the distribution of DO. Above 2 -3 mg $l^{-1}$, the oxygen depletion near the surface increases
760 approximately linearly with increases in the depth-averaged SSC, depth, organic material
761 decay coefficient, and SOD. Near bed DO concentrations are less than at the surface, and are
762 further reduced by increasing depth or reducing mixing, which hinders the transmission of
763 surface aeration.
764
765 Over the estuary, increases in near bed, upstream directed currents move the ETZ upstream
766 and amplify SSC and oxygen demand, primarily because suspended sediment is distributed
767 over a smaller volume of water. Hence, the non-linear dependency of baroclinic circulation
768 on $H^3$, coupled with the $H^{-1}$ dependance of currents from freshwater discharge, results in a
769 non-linear DO response as depth is changed. Variations in the longitudinal spread of SSC
770 around the maximum, which are set by hydrodynamic parameters, also affect oxygen demand.
771 Increasing the relative amount of SSC near the bed (by increasing $Pe_v = w_s H/K_v$ ) both
772 amplifies the effect of near-bed, upstream currents and alters the distribution of SSC.
773 Therefore, the coupled effect of mixing ($A_v$ and $K_v$) on both circulation and vertical SSC
774 distribution produces a non-linear DO response. Hence, for a turbid estuary, a dominant
775 control on oxygen depletion is the SSC dynamics, rather than the residence time of water or
776 nutrient inputs.
777

778 Both model results and field measurements show a strong seasonal variation in DO
779 concentrations that are caused both by temperature induced variation in the decay rates of
780 organic material (ie., changing $k_r$ and $S_b$) and oxygen saturation, and by variation in the
781 hydrologic cycle which typically produces low discharge—and high organic material
782 concentrations—during the summer months. This seasonal cycle has been altered by
783 deepening the River Ems from 5 m to 7 m, which has moved the ETZ upstream and amplified
784 SSC. Thus, anthropogenically driven changes to the sediment dynamics explain the reduction
785 in average summertime DO by as much as 2 - 3 mg $l^{-1}$ over the past several decades, and the
786 much greater occurrence of hypoxic events.
787
788

**Acknowledgments**

Many thanks to Verena Brauer, Robbert Schippers, Karin Huijts, Marcel van Maarseveen, and Frans Buschman for logistical support during experiments. Thanks also to Martin Krebs and Helge Juergens from WSA Emden, Rewert Wurpts, Uwe Boekhoff and Baerbel Amman from Niedersachsen Ports (NP), Andreas Engels from NLWKN, and Christine Habermann from the Bundesanstalt fuer Gewaesserkunde (BfG). Andreas Scholl of BfG is especially thanked for his extensive personal communication. The crews of the Delphin (NP) and the WSA Friesland are also thanked. This work was funded by LOICZ project 014.27.013 (Land Ocean Interaction in the Coastal Zone), and administered by NWO-ALW, the Netherlands Organization for Scientific Research.

## 7. References

APHA. 1992. *Standard methods for the examination of water and wastewater*, 18 ed. American Public Health Association, American Waterworks Association, Water Environment Federation.

Baretta, J.W. and P. Ruardij (eds.), 1988. *Tidal flat estuaries: Simulation and Analysis of the Ems Estuary*. Ecological Studies 71. Springer Verlag. 353 pp.

Benoit, P., Y. Gratton, and A. Mucci. 2006. Modeling of dissolved oxygen levels in the bottom waters of the Lower St. Lawrence Estuary: Coupling of benthic and pelagic processes. *Marine Chemistry* 102:13–32. doi:10.1016/j.marchem.2005.09.015.

van Beusekom, J.E.E. & V.N. de Jonge, 1998. Retention of phosphorus and nitrogen in the Ems estuary. *Estuaries*, 21: 527-539.

Borsuk, M.E., C.A. Stow, R.A. Luettich, Jr., H.W. Paerl, and J.L. Pinckney. 2001. Modelling oxygen dynamics in an intermittently stratified estuary: Estimation of process rates using field data, *Estuarine, Coastal and Shelf Science* 52:33–49.

Chapra S.C. 1997. *Surface water-quality modeling*. McGraw-Hill International editions.

Colijn, F., 1982. Light absorption in the waters of the Ems-Dollard estuary and its consequences for the growth of phytoplankton and microphytobenthos. *Netherlands Journal of Sea Research* 15: 196-216.

Cox, B.A. 2003. A review of dissolved oxygen modeling techniques for lowland rivers. *The Science of the Total Environment* 314 –316:303–334. doi:10.1016/S0048-9697(03)00062-7.

Dai, M., X. Guo, W. Zhai, L. Yuan, B. Wang, L. Wang, P. Cai, T. Tang, and W.J. Cai. 2006. Oxygen depletion in the upper reach of the Pearl River estuary during a winter drought. *Marine Chemistry* 102**:**159–169. doi:10.1016/j.marchem.2005.09.020.

Diaz, R.J., and R. Rosenberg. 1995. Marine benthic hypoxia: A review of its ecological effects and the behavioral responses of benthic macrofauna. *Oceanography and Marine and Biology: An Annual Review* 33:245–303.

Engle, V.D., J.K Summers., and J.M. Macauley. 1999. Dissolved oxygen conditions in northern Gulf of Mexico estuaries. *Environmental Monitoring and Assessment* 57:1–20.

van Es, F.B, M.A. van Arkel, L.A. Bouwman and H.G.J. Schröder, 1980. Influence of organic pollution on bacterial macrobenthic and meiobenthic populations in intertidal flats of the Dollard. *Netherlands Journal of Sea Research* 14: 288-304.

Essink, K., 2003. Response of an estuarine ecosystem to reduced organic waste discharge. *Aquatic Ecology* 37(1): 65-76

Fang, T.H., and C.L. Lin. 2002. Dissolved and particulate trace metals and their partitioning in a hypoxic estuary: The Tanshui Estuary in northern Taiwan. *Estuaries* 25:598–607.

Friedrichs, C.T., Armbrust, B.D., & de Swart, H.E., 1998. Hydrodynamics and equilibrium sediment dynamics of shallow, funnel-shaped tidal estuaries. In *Physics of Estuaries and Coastal Seas* Dronkers, eds. J. Dronkers, and M.B.A.M. Scheffers, 315–327. Rotterdam: Balkema.

Garban, B., D. Olivon, M. Poulin, V. Gaultier, and A. Chesterikoff. 1995. Exchanges at the sediment-water interface in the river Seine, downstream from Paris. *Water Research* 29:473–481.

Garnier, J., P. Servais, G. Billen, M. Akopian, and N. Brion. 2001. Lower Seine River and estuary (France) carbon and oxygen budgets during low flow. *Estuaries* 24:964–976.

Hagy, J. D., III, W. R. Boyton, C. W. Keefe, and K. V. Wood. 2004. Hypoxia in Chesapeake Bay, 1950–2001: Long-term change in relation to nutrient loading and river flow. *Estuaries* 27: 634–658.

Hagy, J.D., and M.C. Murrell. 2007. Susceptibility of a northern Gulf of Mexico estuary to hypoxia: An analysis using box models. *Estuarine, Coastal and Shelf Science* 74: 239–253. doi:10.1016/j.ecss.2007.04.013.

Hansen, D.V., and M. Rattray Jr. 1965. Gravitational circulation in straits and estuaries. *Journal of Marine Research* 23:104–122.

Helder, W. and P. Ruardij, 1982. A one-dimensional mixing and flushing model of the Ems-Dollart estuary: calculation of time scales at different river discharges. *Netherlands Journal of Sea Research* 15: 293-312.

de Jonge, V.N. 2000. Importance of temporal and spatial scales in applying biological and physical process knowledge in coastal management, an example for the Ems estuary. *Continental Shelf Research* 20:1655–1686.

de Jonge, V.N. & L.A. Villerius, 1989. Possible role of carbonate dissolution in estuarine phosphate dynamics. *Limnology and Oceanography* 34: 332-340.

887 Jensen, J., C. H. Mudersbach, and C. Blasi. 2003. Hydrological changes in tidal estuaries due
888 to natural and anthropogenic effects. In *Proceedings of the 6. International MEDCOAST 2003*
889 *Conference*, Ravenna, Italy.
890
891 Kineke, G.C., and R.W. Sternberg. 1992. Measurements of high-concentration suspended
892 sediments using the optical backscatter sensor. *Marine Geology* 108:253–258.
893
894 Krebs, M., and H. Weilbeer, 2008. Ems Dollart Estuary. *Die Küste* 74.
895
896 Lin, J., L. Xie, L.J. Pietrafesa, J. Shen, M.A. Mallin, and M.J. Durako. 2006. Dissolved
897 oxygen stratification in two micro-tidal partially-mixed estuaries. *Estuarine, Coastal and*
898 *Shelf Science* 70:423–437. doi:10.1016/j.ecss.2006.06.032.
899
900 Lung, W.S., and A.J. Nice. 2007. Eutrophication Model for the Patuxent Estuary: Advances in
901 Predictive Capabilities. *Journal of Environmental Engineering* 133:917–930.
902 doi:10.1061/(ASCE)0733-9372(2007)133:9(917).
903
904 May, C.L., J. Koseff, L.V. Lucas, J.E. Cloern, D.H. Schoellhamer, 2003. Effects of spatial and
905 temporal variability of turbidity on phytoplankton blooms. *Marine Ecology Progress* Series
906 254, 111–128.
907
908 Monismith, S.G., W Kimmerer, J.R Burau, and M.T. Stacey. 2002. Structure and flow-
909 induced variability of the subtidal salinity field in Northern San Francisco Bay. *Journal of*
910 *Physical Oceanography* 32:3003–3019.
911
912 Munk, W. H., and E.R. Anderson. 1948. Notes on a theory of the thermocline. *Journal of*
913 *Marine Research* 7:276–295.
914
915 Ni, J., L. Sun, and W. Sun. 2007. Modification of chemical oxygen demand monitoring in the
916 Yellow River, China, with a high content of sediments. *Water Environment Research*
917 79:2336–2342. doi:10.2175/106143007X183790.
918
919 Nestlerode, J.A., and R.J. Diaz. 1998. Effects of periodic environmental hypoxia on predation
920 of a tethered polychaete, Glycera americana: implications for trophic dynamics. *Marine*
921 *Ecology Progress Series* 172:185–195.
922
923 Odd, N.V.M. 1988. Mathematical modeling of mud transport in estuaries. In *Physical*
924 *Processes in Estuaries*, eds. J. Dronkers, and W. van Leussen, 503–531. Berlin: Springer
925 Verlag.
926
927 Officer, C.B., 1976. *Two dimensional density gradient flow*. In: Physical oceanography of
928 estuaries (and associated coastal waters): 125-129. New York: Wiley.
929
930 Talke, S.A., H.E. de Swart, and H.M. Schuttelaars. 2009. Feedback between residual
931 circulations and sediment distribution in highly turbid estuaries: An analytical model.
932 *Continental Shelf Research* 29:119–135. doi:10.1016/j.csr.2007.09.002.
933
934 Talke, S.A., H.E. de Swart, and H.M.Schuttelaars. 2008. An analytical model for the
935 equilibrium distribution of sediment in an estuary. In *River, coastal and estuarine*

*morphodynamics*, eds. C.M. Dohmen-Janssen, and S.J.M.H. Hulscher, 403–412. London: Taylor & Francis.

Thouvenin, B., P. Le Hir, and L.A. Romana. 1994. Dissolved oxygen model in the Loire Estuary. In *Changes in fluxes in estuaries, implications from science to management*, eds. K.R. Dyer, and R.J. Orth, 169–178. Fredensborg: Olsen and Olsen.

Uncles, R.J., I. Joint, and J.A. Stephens. 1998. Transport and retention of suspended particulate matter and bacteria in the Humber-Ouse Estuary, United Kingdom, and their relationship to hypoxia and anoxia. *Estuaries* 21:597–612.

Warner, J.C., W.R. Geyer, and J.A. Lerczak. 2005. Numerical modeling of an estuary: A comprehensive skill assessment. *Journal of Geophysical Research* 110**,** CO50001. doi:10.1029/2004JC002691.

Wei, H., Y. He, Q. Li, Z. Liu, and H. Wang. 2007. Summer hypoxia adjacent to the Changjiang Estuary. *Journal of Marine Systems* 67:292–303. doi:10.1016/j.jmarsys.2006.04.014.

Wurpts, R., and P. Torn. 2005. 15 Years experience with fluid mud: Definition of the nautical bottom with rheological parameters. *Terra et Aqua* 99:22–32.

## Appendix

The functions $k_1$ and $k_2$ produce the vertical structure of currents driven by salinity gradients and turbidity gradients, respectively (Eq. 5) and depend on the vertical coordinate $\zeta = z/H$ and the sediment Peclet number $Pe_v = w_s H/K_v$.

$$k_1(\zeta) = (1 - 9\zeta^2 - 8\zeta^3), \tag{A.1}$$

$$k_2(\zeta, Pe_v) = 12G_1 Pe_v^{-4} exp\big(-Pe_v(1+\zeta)\big), \tag{A.2}$$

where $G_1$ is defined as

$$G_1 = 4Pe_v + 6\left(-1 + \frac{1}{3}Pe_v + \zeta^2 - Pe_v\zeta^2\right)exp\big(Pe_v(1+\zeta)\big) + (1+\zeta)exp(Pe_v\zeta)\,\{6 - 6\zeta + (1+3\zeta)Pe_v^2\}. \tag{A.3}$$

The expressions $T_s$, $T_t$, $T_Q$, and $T_K$ in Eqs. 13-15 are defined as follows:

$$T_S = \int_{-1}^{0} k_1(\zeta)exp\big(-Pe_v(\zeta+1)\big)d\zeta, \tag{A.4}$$

$$T_T = \int_{-1}^{0}(1-\zeta^2)exp\big(-Pe_v(\zeta+1)\big)\,d\zeta, \tag{A.5}$$

$$T_Q = \int_{-1}^{0} k_2(\zeta, Pe_v) exp\big(-Pe_v(\zeta+1)\big) d\zeta, \quad \text{(A.6)}$$

$$T_{K_h} = \int_{-1}^{0} exp\big(-(\zeta+1)Pe_v\big) d\zeta\,. \quad \text{(A.7)}$$

Solving, these expressions reduce to functions of the sediment Peclet number $Pe_v$:

$$T_s = \frac{1}{Pe_v^4}\{(-48 + Pe_v^3 - 18Pe_v) exp(-Pe_v) + 48 - 30Pe_v + 6Pe_v^2\}, \quad \text{(A.8)}$$

$$T_T = 144 G_2 Pe_v^{-7} exp(-2Pe_v)\,, \quad \text{(A.9)}$$

$$G_2 = -1 + \frac{1}{12}Pe_v^4 + Pe_v^2 + \frac{1}{2}Pe_v^3 + \left(-2Pe_v - Pe_v^2 + \frac{1}{3}Pe_v^3 + 2\right)\exp(Pe_v) + \left(-1 - Pe_v^2 + \frac{1}{6}Pe_v^3 + 2Pe_v\right)\exp(2Pe_v), \quad \text{(A.10)}$$

$$T_Q = \frac{-2}{Pe_v^3}\left\{1 - Pe_v + \left(-1 + \frac{1}{2}Pe_v^2\right) exp(-Pe_v)\right\}, \quad \text{(A.11)}$$

$$T_{K_h} = \frac{1 - exp(-Pe_v)}{Pe_v}\,. \quad \text{(A.12)}$$

999 **Figures**
1000

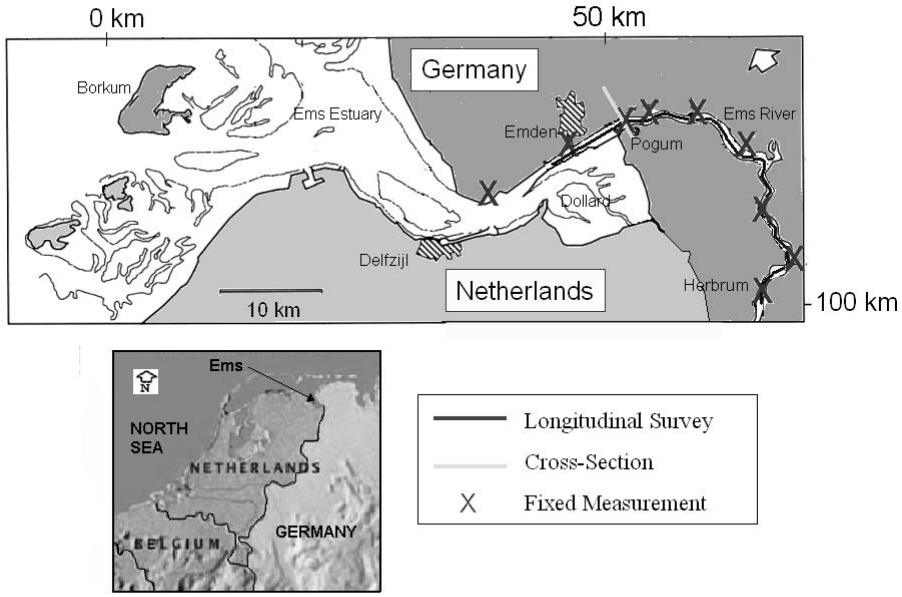


1001

1002 Figure 1: Map of the Ems-Dollard estuary. Location of the longitudinal transect between
1003 Emden and Herbrum is shown, along with the location of a cross-sectional cruise near Pogum.
1004 The locations of long-term monitoring stations by the NLWKN are shown with an 'X'.
1005 Moving downstream from Herbrum, these stations are: (a) Herbrum (km 100), (b) Papenburg
1006 km 86.9, (c) Weener (km 80.4), (d) Leerort (km 72.6), (e) Terborg (km 62.7), (f) Gandersum
1007 (km 55.6), (g) Pogum (km 52), (h) Emden (km 46.1), and (i) Knock (km 36.4). The Dollard
1008 is separated from the main channel of the Ems river by a semi-porous dike (the 'Geisedam').
1009

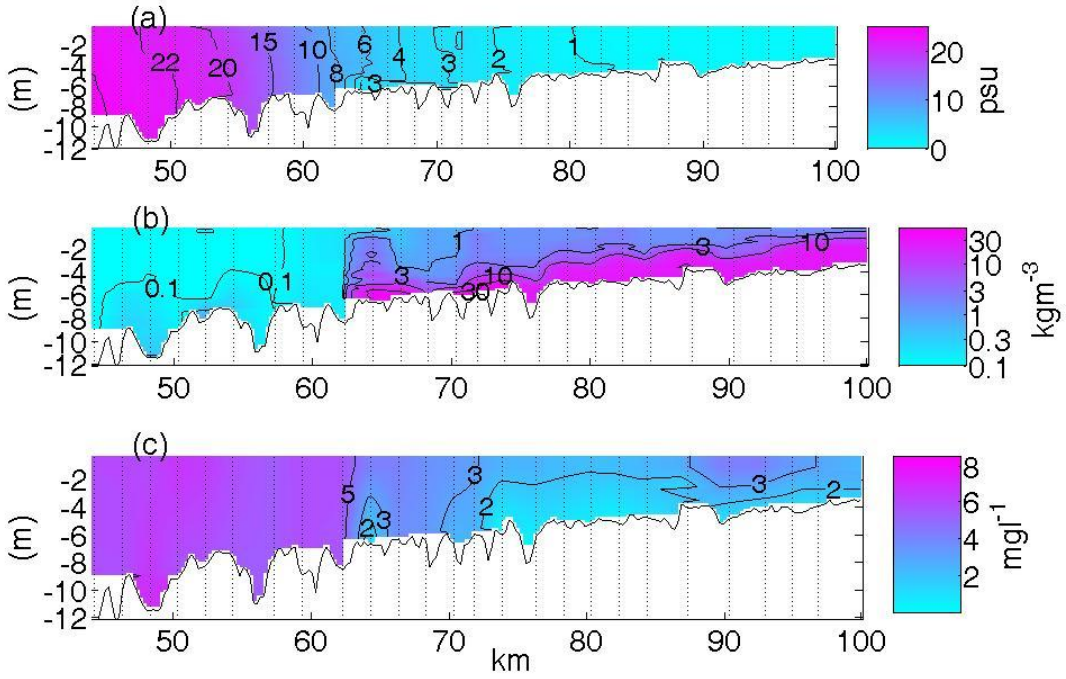


Fig. 2: Salinity (a), SSC (b), and dissolved oxygen concentration (c) as a function of depth below the surface along the longitudinal axis of the Ems estuary (km from North Sea) during the ebb of Aug. 2, 2006. Results are interpolated between 25 casts of the CTD/OBS/oxygen sensor, whose locations are shown by vertical dotted lines. The plots of salinity and SSC are reproduced from Talke et al., (2009).

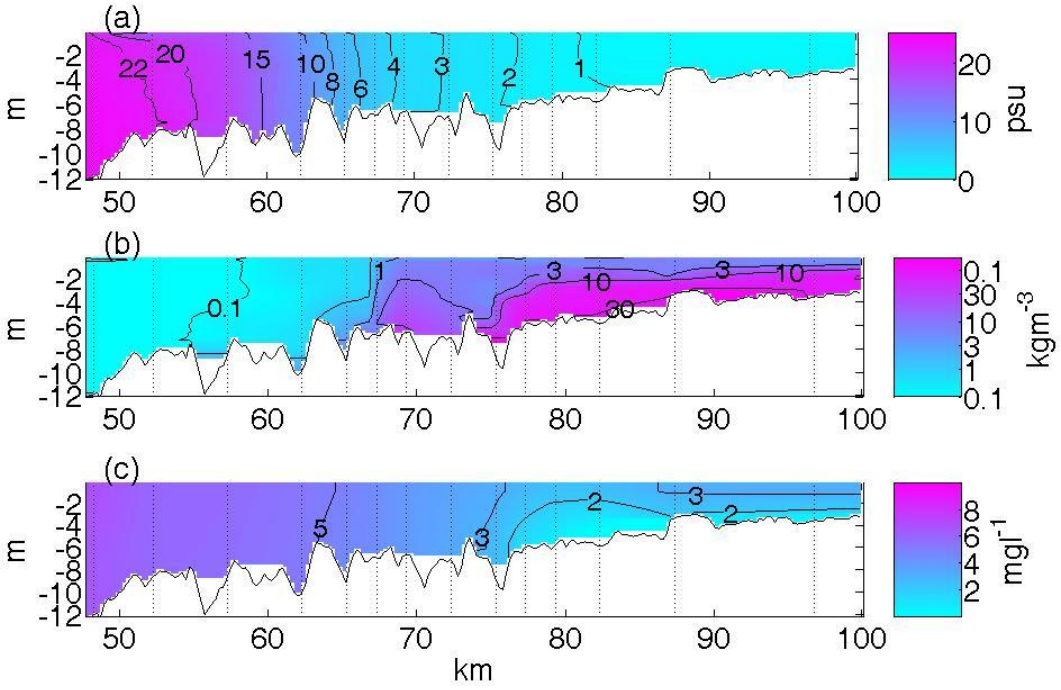


Figure 3: Salinity (a), SSC (b) and dissolved oxygen concentration (c) as a function of depth below the surface and the longitudinal position along the Ems estuary (km from North Sea) during the flood tide on Aug. 2, 2006. Plot follows format of Fig. 3. Differences in bathymetry and water depth between Fig. 2 and Fig. 3 reflect differences in ship course and tidal stage. The salinity and SSC plots are adapted from Talke et al., (2009).

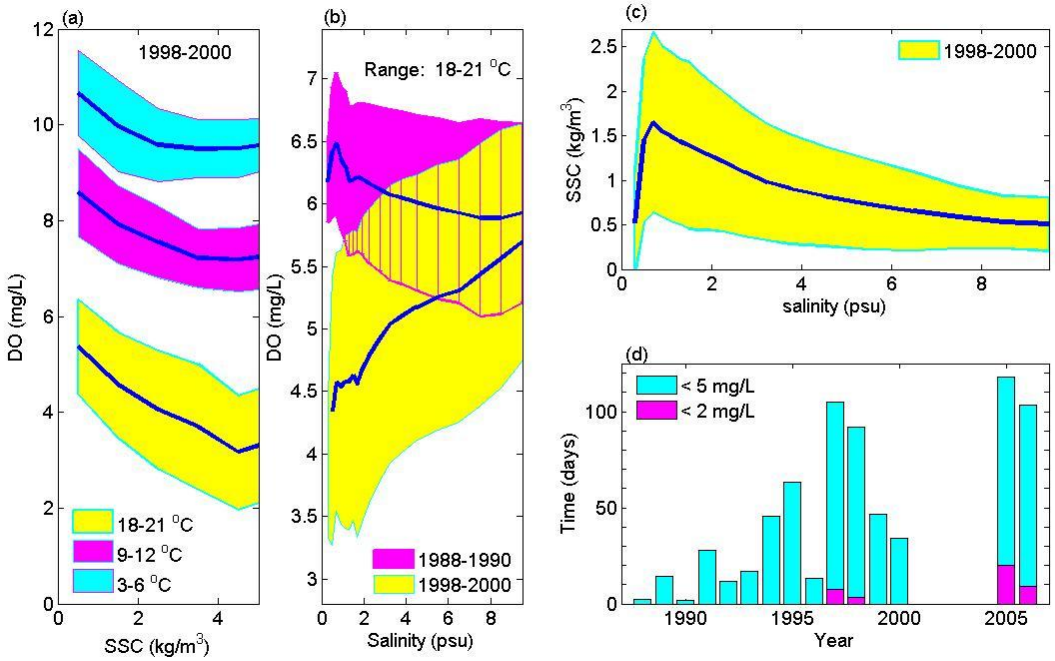


Figure 4: Measurements from the fixed station in Terborg at km 62.7 showing variation in DO vs. SSC for 1998-2000 (a), DO vs. salinity for 1988-1990 and 1998-2000 (b), SSC vs. salinity for 1998-2000 (c), and the time period, measured in days, that DO was below 2 $mgl^{-1}$ and 5 $mgl^{-1}$ (d). The bin-averaged data is depicted by solid lines in (a), (b), and (c), and the standard deviation is depicted with an envelope. For (a) and (b), data was also binned into the depicted temperature ranges. Measurements were collected by the NLWKN at a height of 1.5 m above the bed.

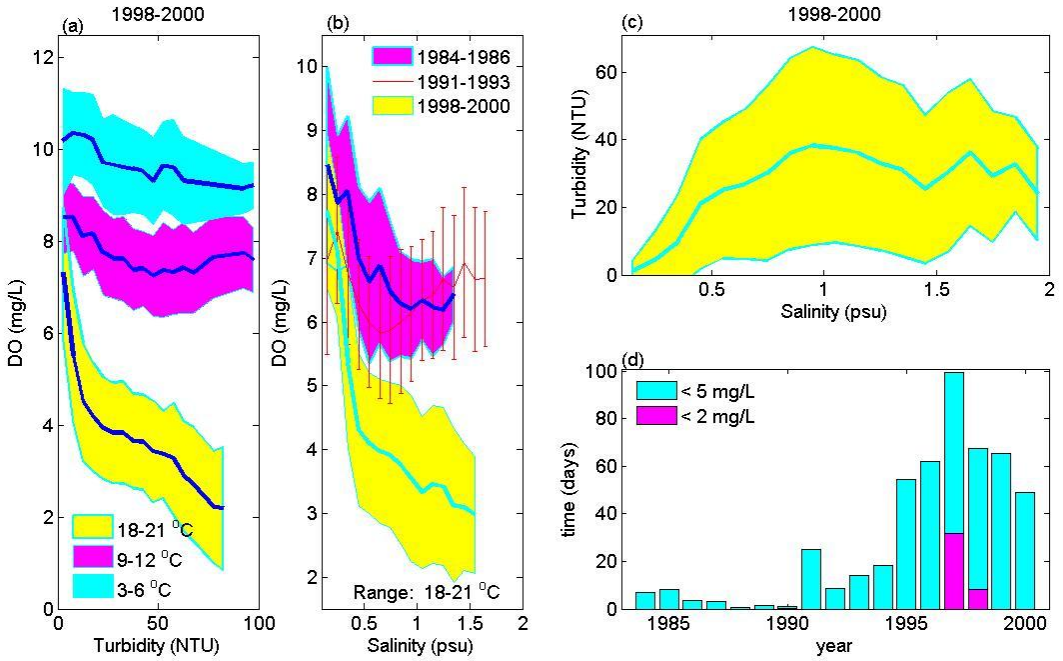


1036

1037 Fig.5: Measurements from the fixed station in Leer-Leda showing variation in DO vs.
1038 turbidity for 1998-2000 (a), DO vs. salinity for 1984-1986, 1991-1993 and 1998-2000 (b),
1039 turbidity vs. salinity for 1998-2000 (c), and the time period, measured in days, that DO was
1040 below 2 $mgl^{-1}$ and 5 $mgl^{-1}$ (d). The bin-averaged data is depicted by solid lines in (a), (b),
1041 and (c), and the standard deviation is depicted with an envelope or bars. For (a) and (b), data
1042 was also binned into the depicted temperature ranges. Measurements were collected by the
1043 NLWKN at a height of 1 m below the water surface. The station is located approximately 3.9
1044 km from the discharge of the Leda into the Ems at km 73.3.

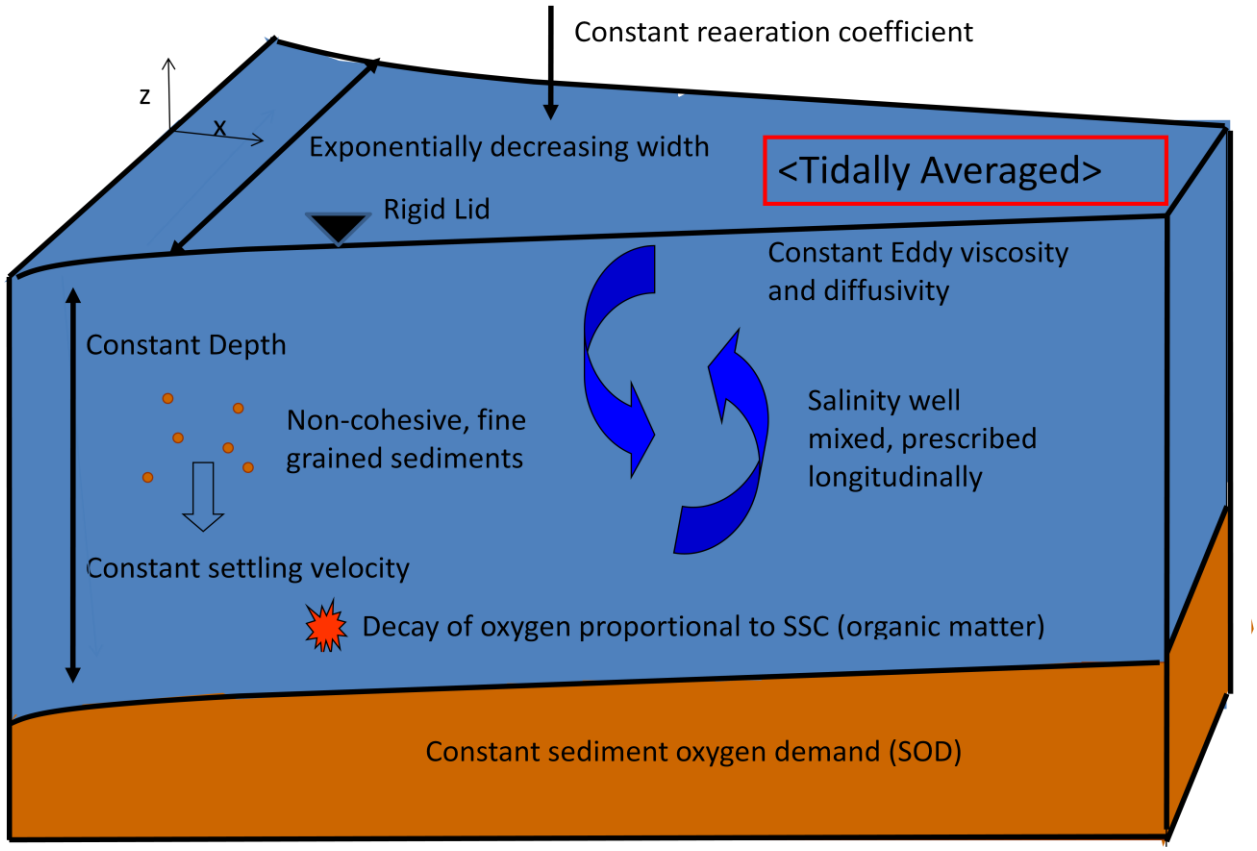


1045

1046 Figure 6: Assumptions made during derivation of model.

1047

1048

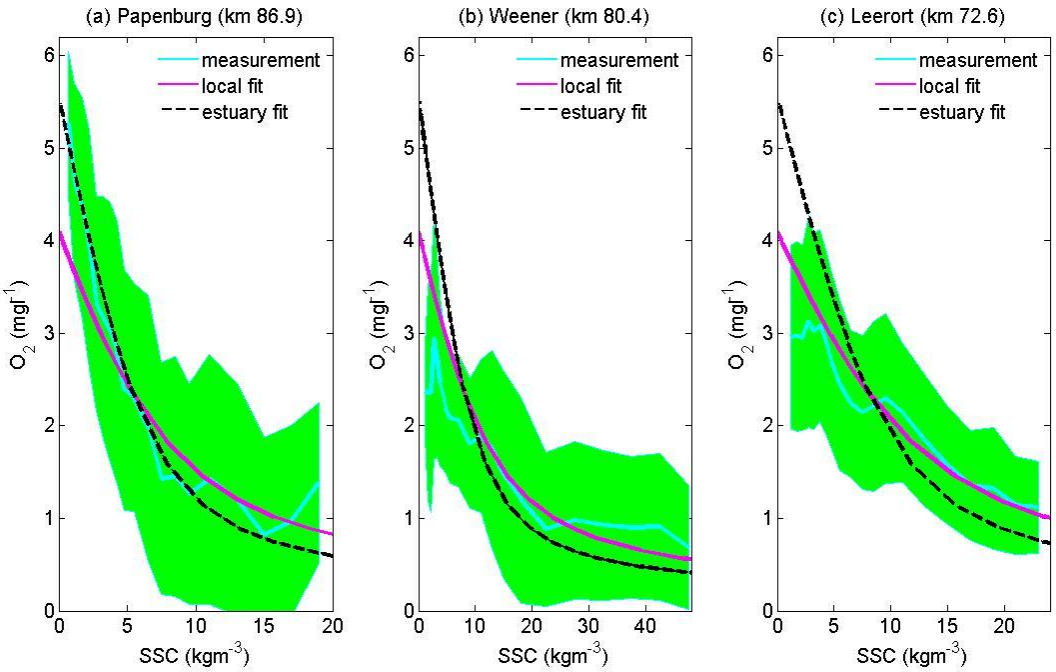


1049

1050 Fig. 7: Measured average DO as a function of measured SSC at 3 stations along the Ems for
1051 the temperature range 18 $^{o}$C to 21 $^{o}$C for data from 2005-2006, compared with 1D model
1052 results. The standard deviation of the measurement is shown by the envelope around the
1053 mean. Two parameter fits are depicted: a 'local' fit that minimizes error in Weener (b) and
1054 Leerort (c), and an 'estuary fit' that better represents average DO over the estuary in the limit
1055 of zero SSC.

1056

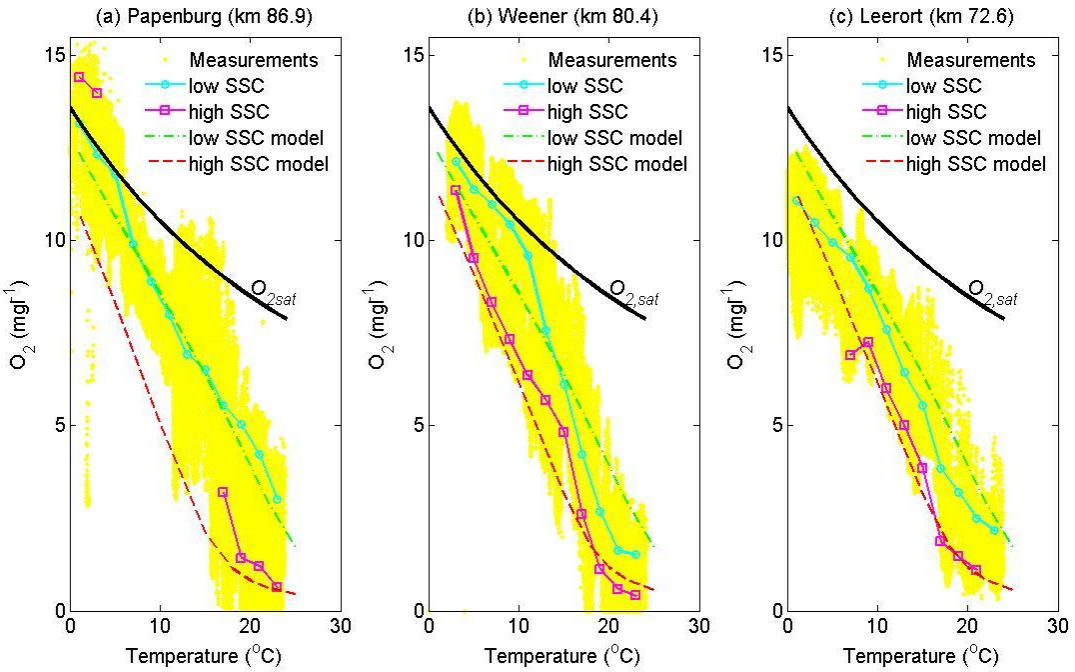


Fig. 8: Variation in measured DO as a function of temperature, compared with 1D model results. A scatter plot of measurements shows total variation of data from 2005-2006. Saturated conditions are shown by a solid black line. 'Low SSC' and 'high SSC' measurements correspond to average DO from SSC bins of 0-1 $kgm^{-3}$ and 18-25 $kgm^{-3}$, respectively. "Low SSC model" and "high SSC model' correspond to a modeled SSC of 0.5 $kgm^{-3}$ and 20 $kgm^{-3}$ at the measurement heights of 2 m, 1.5m , and 1.5 m for Figs. a,b, and c, respectively. The parameters corresponding to the local fit to the turbid zone were used, and a temperature adjustment coefficient of $\theta = 1.1$ was used. Saturated DO concentrations are depicted with a solid black line.

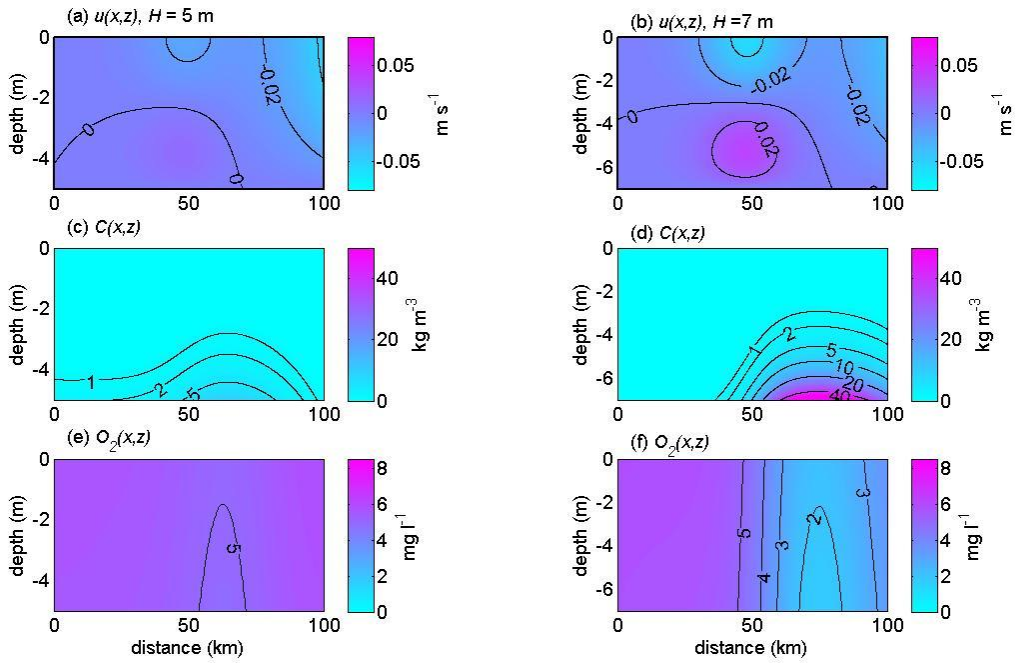


Figure 9: Variation in modeled circulation (top panels), SSC (middle panels), and dissolved oxygen concentrations (bottom panels) when changing depth from 5 m (left panels) to 7 m (right panels). All other parameters are set to the standard values in Table 2.

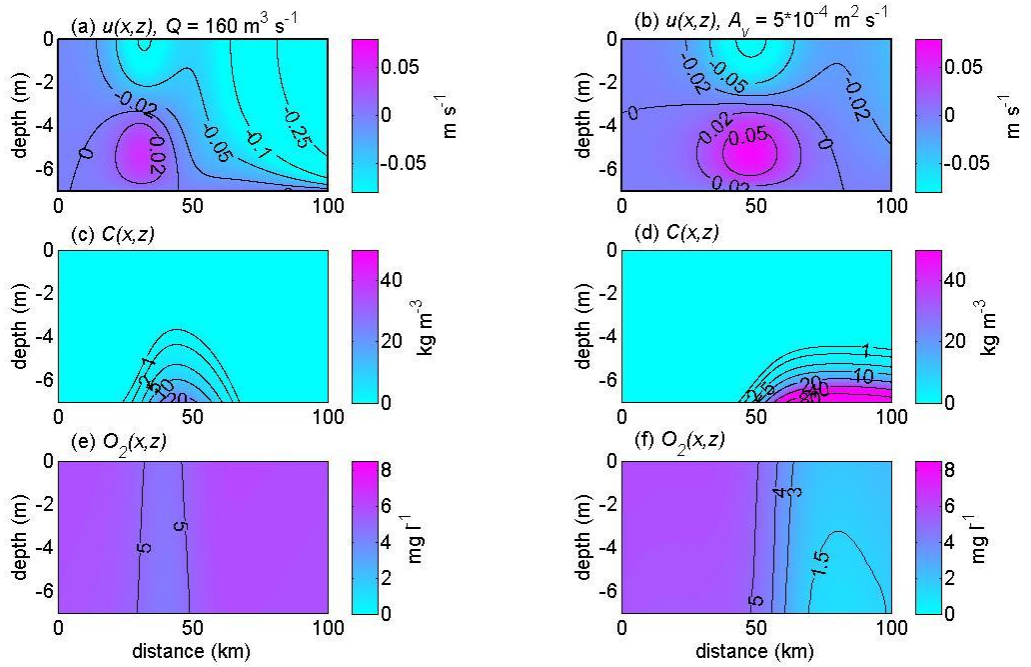


Figure 10: Variation in modeled circulation (top panels), SSC (middle panels), and oxygen concentrations (bottom panels) for a discharge of 160 $m^3 s^{-1}$ (a,c,e) and an eddy viscosity and eddy diffusivity of 0.0005 $m^2 s^{-1}$ (b,d,f). All other parameters are set to the standard values in Table 2.

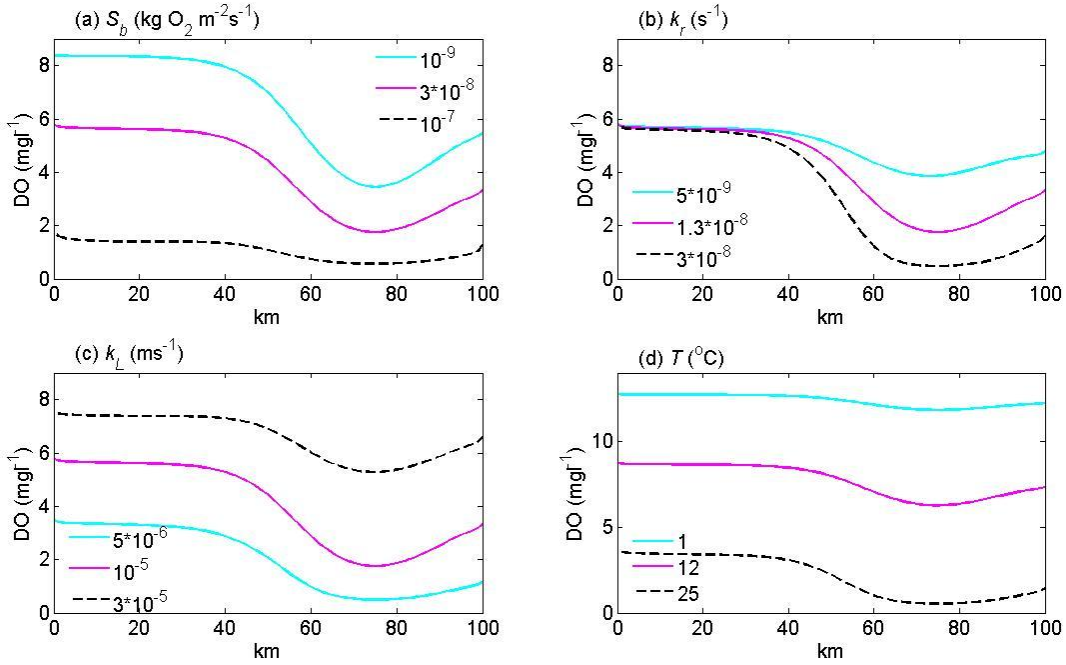


Figure 11: Sensitivity in the modeled longitudinal profile of bottom ($z$ = -$H$) DO concentration to prescribed variations in sediment oxygen demand $S_b$ (11a), suspended sediment oxygen demand $k_r$ (11b), aeration $k_L$ (11c) and temperature $T$ (11d). The SSC profile for each case is found used the standard parameters in Table 2. The solution using the standard DO parameters in Table 1 is given by the solid magenta (dark shaded) profile in 11a, 11b, and 11c.

1093 Table 1: Variation of salinity parameters $x_L$ (length scale of salinity variation), $x_c$ (location of
1094 maximum gradient), the maximum magnitude of the salinity gradient $ds/dx_{max}$, and the
1095 position of the 2 psu isohaline $X_2$ as a function of freshwater discharge $Q$. These results are
1096 found from an equilibrium fit to available long-term data, using the method described in
1097 Monismith et al. (2002). Units of length are in $10^3$ m.

| $Q$ ($m^3s^{-1}$) | -10 | -20 | -40 | -60 | -80 | -100 | -160 | -240 | -320 | -600 |
|---|---|---|---|---|---|---|---|---|---|---|
| $x_L$ ($10^3$ m) | 15.7 | 14.2 | 12.7 | 12 | 11.5 | 11 | 10.3 | 9.7 | 9.3 | 8.4 |
| $x_c$ ($10^3$ m) | 47.9 | 43.1 | 38.7 | 36.4 | 34.9 | 33.7 | 31.4 | 29.5 | 28.2 | 25.6 |
| $ds/dx_{max}$ | 0.0095 | 0.0011 | 0.0012 | 0.00125 | 0.0013 | 0.00135 | 0.00145 | 0.00155 | 0.0016 | 0.0018 |
| $X_2$ ($10^3$ m) | 67.1 | 60.4 | 54.3 | 51.1 | 48.9 | 44.0 | 41.3 | 39.6 | 39.6 | 36.0 |

1098

1099 Table 2: Standard parameters prescribed in the vertical model of oxygen depletion (Section
1100 4.1): $K_v$= eddy diffusivity, $H$ = depth, $w_s$ = settling velocity, $k_L$ = aeration coefficient, $S_b$ =
1101 bottom oxygen demand, $k_r$ = oxygen demand due to SSC, $p$ = proportion of SSC that is
1102 organic matter, $T$ = water temperature.

| | $K_v$ ($m^2s^{-1}$) | $H$ (m) | $w_s$ ($ms^{-1}$) | $k_L$ ($ms^{-1}$) | $S_b$ (kg $O_2$ $m^{-2}$ $s^{-1}$) | $k_{ref}$ ($s^{-1}$) | $p$ ( - ) | $T$ ($^oC$) |
|---|---|---|---|---|---|---|---|---|
| **'local fit'** | 0.001 | 7 | 0.001 | $10^{-5}$ | $5\times10^{-8}$ | $8\times10^{-9}$ | 0.1 | 20 |
| **'estuary fit'** | 0.001 | 7 | 0.001 | $10^{-5}$ | $3\times10^{-8}$ | $1.3\times10^{-8}$ | 0.1 | 20 |

1103

1104

1105

1106

Table 3: Standard parameters used to calculate circulation and the equilibrium distribution of sediment in the 2D model. The standard depth $H$, settling velocity $w_s$, and eddy diffusivity $K_v$ are described in Table 2, as are the additional parameters needed for the oxygen model—$k_L$, $k_r$, p, and $S_b$. Here, $S_*$ is the salinity at the seaward boundary, $x_L$ scales the salinity gradient, $x_c$ is the location of the maximum salinity gradient relative to the seaward boundary, $A_v$ = eddy viscosity, $L$ = length of model domain, $Q$ = freshwater discharge, $K_h$ = horizontal dispersion coefficient, $c_*$ is the average SSC over the estuary, $L_e$ is the convergence length-scale, and $B_o$ is the width at the estuarine mouth . Note that discharge $Q$ is negative in our coordinate system.

| $S_o$ (psu) | $x_L$ (m) | $x_c$ (m) | $A_v$ ($m^2s^{-1}$) | L (m) | $Q$ ($m^3s^{-1}$) | $K_h$ ($m^2s^{-1}$) | $c_*$ ($kgm^{-3}$) | $L_e$ (m) | $B_o$ (m) |
|---|---|---|---|---|---|---|---|---|---|
| 30 | $14\cdot10^3$ | $43\cdot10^3$ | 0.001 | $100\cdot10^3$ | -10 | 100 | 0.5 | $20\cdot10^3$ | $8\cdot10^3$ |

# An idealized model and systematic process study of oxygen depletion in highly turbid estuaries

S.A. Talke[1], H.E. de Swart[2], V.N.de Jonge[3]

(1): Civil & Environmental Engineering Department, University of Washington
201 More Hall, Box 352700
Seattle, WA 98195-2700 USA
e-mail: stalke@u.washington.edu

(2): Institute for Marine and Atmospheric research, Utrecht University,
Princetonplein 5, 3584 CC Utrecht, the Netherlands
e-mail: h.e.deswart@uu.nl

(3): Institute of Estuarine Coastal Studies (IECS), University of Hull
Hull, HU6 7RX, United Kingdom
e-mail: v.n.de.jonge@planet.nl

## Supplement S1: Model Derivation

In this supplement we derive our circulation and sediment transport models, first presented in Talke et al. (2008, 2009) and repeated here for the convenience of the reader.

## Circulation Model

We begin by constructing an expression for tidally averaged momentum, defining the *x*-axis to be pointed upstream in the along-estuary direction, the *z*-axis to be pointed vertically upward from the undisturbed water surface, and the *y*-axis to be pointed transversely from the estuarine centerline. Velocity components along the *x* and *z* axes are *u* and *w*, respectively. Both water depth *H* and eddy viscosity $A_v$ are assumed constant over the model domain, and the rigid lid approximation is imposed. The width *b* is assumed to vary smoothly with an exponential decay, and is defined from the observed width of the Ems estuary such that $b(x) = B_o \exp\left(-x/L_e\right)$, where $B_o$ is the width of the estuary at the inlet ($x$=0) and $L_e$ is the e-folding scale. Density, velocity, and surface slope are assumed to be constant in the *y*-direction. Nonlinear terms such as $u\,\partial u/\partial x$ and $w\partial u/\partial z$ are neglected because of their small magnitude in a tidally averaged

system. Using the shallow water approximation, the tidally averaged, width averaged momentum equation in the horizontal direction is:

$$0 = -\frac{\partial p}{\partial x} + \frac{\partial}{\partial z}\left\{\rho_o A_z \frac{\partial u}{\partial z}\right\}, \tag{S1.1}$$

where $p$ is pressure and $\rho_o$ is a reference density (water). In the vertical direction we assume a hydrostatic balance,

$$\frac{\partial p}{\partial z} = -\rho g, \tag{S1.2}$$

where $g$ is gravity [m s$^{-2}$] and $\rho$ is the density [kg m$^{-3}$]. Integrating Eq. S1.2, and substituting into the pressure term in Eq. S1.1 yields

$$0 = -g\int_z^0 \frac{\partial \rho}{\partial x} dz' - g\rho_o \frac{d\eta}{dx} + \frac{\partial}{\partial z}\left\{\rho_o A_v \frac{\partial u}{\partial z}\right\}, \tag{S1.3}$$

where $d\eta/dx$ is the surface slope [-]. The no-slip condition is applied at the bottom boundary ($u = 0$ at $z = -H$) and momentum flux from wind-shear is assumed to be vanishingly small at the water surface ( $\rho_o A_v \frac{\partial u}{\partial z} = 0$ at $z = 0$). Circulation is thus defined as a balance between baroclinic forcing (term 1), the barotropic surface slope (term 2), and mixing (term 3). Baroclinic forcing is defined by the longitudinal density gradient, which is a function of both salinity $s(x)$ and the suspended sediment concentration $C(x,z)$:

$$\frac{\partial \rho}{\partial x} = \beta \frac{ds(x)}{dx} + \gamma \frac{\partial C(x,z)}{\partial x}. \tag{S1.4}$$

The factor ß ~ 0.83 kg/m$^3$/psu and the relative density of sediment, $\gamma = (\rho_s - \rho_o)/\rho_s \sim 0.62$ convert salinity and SSC into density, where $\rho_s$ is the density of fine-grained, non-cohesive sand particles with a single grain size and a density of 2650 kg/ m$^3$. The salinity gradient is applied diagnostically as described in Eq. 3 of the main text and supplement S2, while the longitudinal SSC distribution and gradient is solved by the model. The vertical structure of SSC is found by assuming that the flux of sediment due to upwards diffusion is balanced by the flux caused by a

constant downwards settling velocity, and yields an exponential profile (see Eq. 4 of the main text and supplement S2).

Next we apply the mass balance condition for water, which requires that a prescribed freshwater discharge $Q$ [m$^3$/s] must equal the tidally averaged flow of water through a cross-section:

$$b(x)\int_{-H}^{0} u(x,z)dz = Q \tag{S1.5}$$

where $u(x,z)$ is the tidally averaged current . Because the $x$-axis is oriented in the upstream direction, the discharge $Q$ is a negative quantity in the present coordinate system. The tidally averaged current structure as a function of the surface gradient $d\eta/dx$ is determined by integrating Eq. S1.3 twice in the vertical and applying the surface and bed boundary conditions. The surface gradient d$\eta/dx$ is solved by applying the mass balance equation, S1.5. Solving yields the tidally averaged circulation equation described below (see also Eq. 5 of the main text):

$$u(x,\zeta) = \underbrace{\frac{g\beta H^3}{48\rho_o A_v}k_1(\zeta)\frac{ds}{dx}}_{baroclinic\ circulation} + \underbrace{\frac{g\gamma H^3}{48\rho_o A_v}k_2(\zeta, Pe_v)\frac{dc_b}{dx}}_{SSC\ induced\ circulation} + \underbrace{\frac{3Q}{2b(x)H}(1-\zeta^2)}_{freshwater\ circulation}, \tag{S1.6}$$

where $\zeta = z/H$ is the non-dimensional height, $g$ is gravity, $Q$ is the freshwater discharge, $c_b(x)$ is the variation in bottom SSC, and $Pe_v = w_s H / K_v$ is the vertical Peclet number for SSC. The functions $k_1$ and $k_2$, which are found during integration, are defined in the appendix of the main text.

**Sediment Concentration and Morphodynamic Equilibrium**

The remaining unknown, the horizontal variation in the bottom SSC, $c_b(x)$, is found using the condition of morphodynamic equilibrium. For simplicity we start with the full equation for sediment mass balance,

$$0 = \frac{-\partial}{\partial x}\{b(x)C(x,z)u(x,z)\} - \frac{\partial}{\partial z}\{b(x)C(x,z)w(x,z) - w_s\} + \frac{\partial}{\partial x}\left\{b(x)K_h\frac{\partial C(x,z)}{\partial x}\right\} + \frac{\partial}{\partial z}\left\{b(x)K_v\frac{\partial C(x,z)}{\partial z}\right\}, \quad \text{(S1.7)}$$

where $K_h$ and $K_v$ are the horizontal and vertical diffusion coefficients, and $w_s$ is the settling velocity of sediment. Note that terms involving derivatives with respect to *y* are ignored, as we assume all variables to be independent of *y*. We next apply the boundary condition that there is no flow and no sediment flux through either the top and bottom boundary (at $z = 0$ and $z = -H$)

$$w(x,z)\big|_{z=0.z=-H} = 0, \quad \text{(S1.8a)}$$

$$\left\{w_s C + K_v\frac{\partial C}{\partial z}\right\}\Big|_{z=0} = 0, \quad \text{(S1.8b)}$$

$$\left\{-w_s C - K_v\frac{\partial C}{\partial z}\right\}\Big|_{z=-H} = E - D, \quad \text{(S1.8c)}$$

where $E$ is the erosion and $D$ is the deposition of sediment at the bed. At the upstream boundary of $x=L$, we make the further assumption that the vertically integrated flux of sediment (sediment transport) into the model vanishes,

$$\int_{-H}^{0}\left\{u(x,z)C(x,z)b(x) - K_h b(x)\frac{\partial C(x,z)}{\partial x}\right\}dz\Big|_{x=L} = 0. \quad \text{(S1.9)}$$

We next non-dimensionalize Eq. S1.7 by assuming the following scales:

$$\tilde{x} = \frac{x}{x_L}\ ; \qquad \tilde{z} = \frac{z}{H}; \qquad \tilde{C} = \frac{C}{c_*}; \qquad \tilde{w} = \frac{w}{W_*}; \qquad \tilde{u} = \frac{u}{U_*}; \qquad \tilde{b} = \frac{b}{B_o}, \qquad \text{(S1.10)}$$

where $x_L \sim 10 \cdot 10^3$ m is the length scale of the salinity gradient, $H \sim 10$ m is the depth, $c_*$ is the average bottom sediment concentration, $U_* \sim 0.01$ m/s is the horizontal velocity scale, the vertical velocity scale $W_* = H\,U_*/x_L \sim 10^{-5}$ m/s. The typical magnitude for settling velocity $w_s$ is 0.001 m/s.

From these definitions, we can construct the non-dimensional mass balance equation,

$$0 = \frac{-H^2 U_*}{K_v x_L}\frac{\partial}{\partial \tilde{x}}\{\tilde{u}\tilde{C}\tilde{b}\} - \frac{HW_*}{K_v}\left\{\tilde{C}\tilde{b}\left(\tilde{w} - \frac{w_s}{W_*}\right)\right\} + \frac{H^2 K_h}{K_v x_L^2}\frac{\partial}{\partial \tilde{x}}\left\{\tilde{b}\frac{\partial \tilde{C}}{\partial \tilde{x}}\right\} + \frac{\partial}{\partial \tilde{z}}\left\{\tilde{b}\frac{\partial \tilde{C}}{\partial \tilde{z}}\right\}, \qquad (S1.11)$$

where the terms $c_*$ and $B_o$ drop out because they are present in each term. Assuming that the tidally averaged order of magnitude of $K_h$ and $K_v$ are 100 m$^2$/s and 0.001 m$^2$/s, we find that the order of magnitude of the three scaling terms in Eq. S1.11 are

$$\frac{H^2 U_*}{K_v x_L} \sim 10^{-1}\ ; \qquad \frac{HW_*}{K_v} \sim 10^{-1}; \qquad \frac{H^2 K_h}{x_L^2 K_v} \sim 10^{-1}. \qquad \text{(S1.12)}$$

From this scaling we find that $\partial/\partial\tilde{x}\{-\tilde{u}\tilde{C}\tilde{b}\}$, $\partial/\partial\tilde{z}\{-\tilde{w}\tilde{C}\tilde{b}\}$, and $\partial/\partial\tilde{x}\{\tilde{b}\,\partial\tilde{C}/\partial\tilde{x}\}$ are second order terms. Thus, we conclude that the dominant, leading order balance must be between the terms $\tilde{b}\frac{\partial}{\partial z}\left\{\tilde{C}\frac{\widetilde{w_s}}{W_*}\right\}$ and $\tilde{b}\frac{\partial}{\partial \tilde{z}}\left\{\frac{\partial \tilde{C}}{\partial \tilde{z}}\right\}$. Reverting to dimensional form (Eq. S1.7), the leading order balance reduces to:

$$\frac{\partial}{\partial z}\ Cw_s\ + \frac{\partial}{\partial z}\left\{K_v \frac{\partial C}{\partial z}\right\} = 0 \qquad \text{(S1.13)}$$

Integrating this equation with respect to *z* yields:

$$C(x,z)w_s + K_v \frac{\partial C(x,z)}{\partial z} = B_1 \qquad \text{(S1.14)}$$

where the term $B_1$ is a constant of integration. Using the boundary condition (S1.8b) yields $B_1 = 0$. Integrating again and applying the condition that the sediment concentration at the bed equals $c_b(x)$ produces an exponential profile of SSC in the vertical direction (Eq. 4 of the main text).

To determine the condition of morphodynamic equilibrium, we next integrate the dimensional form of the mass-balance equation (S1.7) with respect to depth. This yields:

$$0 = \frac{\partial}{\partial x}\int_{-H}^{0} \underbrace{\left\{uCb - K_h b \frac{\partial C}{\partial x}\right\}}_{Horizontal\ Flux} dz + \int_{-H}^{0} \frac{\partial}{\partial z} \underbrace{\left\{Cb(w - w_s) - bK_v \frac{\partial C}{\partial z}\right\}}_{Vertical\ Flux} dz, \qquad \text{(S1.15)}$$

where we have pulled the $\partial/\partial x$ term outside of the integral. We next apply conditions S1.8a-S1.8c and assume that the width integrated erosion *E* equals the width integrated deposition *D* at the bed (this is the condition of morphodynamic equilibrium). Under these conditions, the second term in Eq. S1.15 vanishes. Next we integrate the remaining (first) term with respect to *x*, which yields:

$$\int_{-H}^{0} \left\{ uCb - K_h b \frac{\partial C}{\partial x} \right\} dz = B_2 \,, \tag{S1.16}$$

where $B_2$ is a constant of integration. Using the condition that there is no vertically integrated flux of sediment at the upstream model boundary (Eq. S1.9), we find that $B_2$=0. This is equivalent to Eq. 6 in the main text, after integrating Eq. 6 with respect to *y*.

We integrate Eq. S1.16 with respect to *z*, which yields the following differential equation for the longitudinal distribution of suspended sediment, $c_b(x)$

$$\frac{dc_b}{dx} = \frac{-J_1(x)c_b(x)}{J_2 c_b(x) + J_3} \tag{S1.17}$$

The full expressions for $J_1(x)$, $J_2$, and $J_3$, found during integration, are

$$J_1(x) = -T_s \frac{g\beta H^3}{48\rho_o A_v} \frac{ds}{dx}(x) + \frac{3}{2} T_Q \frac{Q}{Hb(x)}, \tag{S1.18}$$

$$J_2 = -T_T \frac{g\gamma H^3}{48\rho_o A_v}, \tag{S1.19}$$

$$J_3 = -T_K K_h, \tag{S1.20}$$

where $J_1(x)$ describes the effect of salinity gradients and freshwater discharge on vertically integrated SSC fluxes, $J_2$ describes the effect of turbidity currents on vertically integrated SSC fluxes, and $J_3$ describes the effect of horizontal dispersion on vertically integrated SSC fluxes. The parameters $T_S$, $T_T$, $T_Q$, and $T_K$ are defined in the appendix of the main text and are functions of the vertical Peclet number for SSC, $Pe_v = w_s H/K_v$. The differential equation in S1.17 is solved by integration, which yields the following implicit relation for bottom concentration as a function of a constant, $A_1$ (see also Eq. 8 of main text):

$$c_b(x) = A_1 \underbrace{exp(F(x))}_{\substack{longitudinal \\ variation}}, \tag{S1.21a}$$

$$F(x) = \underbrace{\frac{-T_s g \beta H^3 s(x)}{48 \rho_o A_v T_K K_h}}_{\substack{baroclinic \\ component}} - \underbrace{\frac{T_T g H^3 c_b(x)}{48 \rho_o A_v T_K K_h}}_{SSC\ component} + \underbrace{\frac{3 T_Q Q L_e}{2 H T_K K_H b(x)}}_{freshwater\ component}, \quad \text{(S1.21b)}$$

The constant $A_1$ is found by defining the total mass of sediment available for resuspension (see also Eq. 7 of main text),

$$c_* HL\langle b \rangle = \int_{-H}^{0} \int_{-b/2}^{b/2} \int_{0}^{L} C(x,z) b(x) dx dy dz, \quad \text{(S1.22)}$$

where $c_*$ represents the average SSC over the model domain and $<b>$ denotes the mean width of the estuary. Combining Eq. 4 of the main text with Eqs. S1.21 and S1.22 yields an expression for $A_1$ (see also Eq. 9 of main text),

$$A_1 = \frac{c_* Pe_v L < b >}{\left(1 - \exp\left(\frac{-w_s H}{K_v}\right)\right) \int_0^L b(x) \exp\left[\int_0^x F(x)\, dx\right] dx}. \quad \text{(S1.23)}$$

As can be observed in Eq. S1.21, the the bottom concentration $c_b(x)$ occurs both in the left hand side (S1.21a) and right hand side (S1.21b) of the relationship. Hence the solution for $c_b(x)$ must be found iteratively, with the difference between the left-hand size and the right hand side of the equation minimized to with-in a tolerance (in our case, 0.1%). In practice, the solution is found by making an initial guess for the constant $A_1$ and function $F(x)$, for example by solving for the simpler, explicit case in which turbidity currents are negligible and the second term in $F(x)$ vanishes. The resulting initial solution for $c_b(x)$ is then used to find new estimates for $A_1$ and $F(x)$, and the process is repeated until the left hand and right hand sides of Eq. S1.21 agree to an acceptable tolerance.

# An idealized model and systematic process study of oxygen depletion in highly turbid estuaries

S.A. Talke[1], H.E. de Swart[2], V.N.de Jonge[3]

(1): Civil & Environmental Engineering Department, University of Washington
201 More Hall, Box 352700
Seattle, WA 98195-2700 USA
e-mail: stalke@u.washington.edu

(2): Institute for Marine and Atmospheric research, Utrecht University,
Princetonplein 5, 3584 CC Utrecht, the Netherlands
e-mail: h.e.deswart@uu.nl

(3): Institute of Estuarine Coastal Studies (IECS), University of Hull
Hull, HU6 7RX, United Kingdom
e-mail: v.n.de.jonge@planet.nl

## Supplement 2: Experimental Data

This supplement presents data and analysis that justifies the functional forms of the tidally averaged longitudinal salinity gradient and the tidally averaged vertical profile of suspended sediment concentration (SSC) used in the circulation and sediment transport models.

Fig. S2.1 displays measured SSC vs. depth over several tidal periods on Feb. 14th and Feb. 15th, 2006, at a fixed location near Pogum (km 54) on Feb. 14th, 2006. SSCs vary from more than 70 kg $m^{-3}$ near the bed to 0.3 $kgm^{-3}$ at the water surface. Casts of optical backscatter (OBS) are calibrated to SSC, and are found to fit well to an exponential profile with a functional form of $C(z) = c_b exp(-r(z+H))$, where $z$ is the vertical coordinate measured upwards from the surface, $H$ is the water depth, $c_b$ is the bottom concentration, and $r$ is a decay coefficient. The average goodness of fit for 21 casts ranged from $R^2 = 0.56$ to $R^2 = 0.97$, with a mean of $R^2 = 0.8$. Assuming that the upwards flux of sediment by mixing is balanced by downwards settling, Talke et al. (2009) show that the decay coefficient $r$ is equal to the ratio of eddy diffusivity ($K_v$) and

settling velocity ($w_s$), or $r = K_v/w_s$. As shown in Fig. S2b, the average ratio is $r$= (0.8 ± 0.3) $m^{-1}$, with the largest values observed during the ebb and slack tides. Thus, to first order, an exponential distribution of SSC in the vertical is reasonable.

The diagnostic longitudinal salinity profile used to drive the analytical circulation model is found from salinity data measured at nine long-term monitoring stations between Knock (km 37) and the tidal weir at Herbrum (km 100) between Feb. 2005 and October 2005, as well as surface measurements of salinity at Borkum (km 0) during monthly cruises from 2005 to 2006. We assume well mixed conditions over a tidal period. The average of 30.2 psu at km 0 is weighted to be of equal size as the fixed station measurements. Using the method described in Monismith et al. (2002), we normalize the location of tidally averaged salinity data by the $X_2$ location, defined as the location at which the tidally averaged salinity is 2 psu. As shown in Fig. S2.2a, this normalization collapses the tidally averaged salinity data to a parametric function of the ratio $x_* = x/X_2$, where $x$ is measured from the estuarine boundary with the North Sea (km 0). The data is then fit to a hyperbolic tangent with the form:

$$s(x_*) = 0.5S_o\left\{1 - \tanh\left(\frac{x_* - x_c^*}{x_L^*}\right)\right\}, \qquad \text{(S2.1)}$$

where $s$ is the salinity, $S_o$ = 30 psu, $x_c^*$ = 0.713, and $x_L^*$ = 0.235. The dimensional values defined in Eq. 3 of the main text are found with $x_c = X_2 x_c^*$ and $x_L = X_2 x_L^*$, respectively. Hence, the longitudinal salinity profile is known if the position of the $X_2$ isohaline is defined.

We next construct an equilibrium relationship between the $X_2$ isohaline and freshwater discharge. Using the measured $X_2$ position and the daily-averaged freshwater discharge $Q$, and following Monismith et al., (2002), we define the following non-linear regression:

$$X_2(t) = aX_2(t-1) + bQ^c, \qquad \text{(S2.2)}$$

where $X_2(t-1)$ is the position of the $X_2$ isohaline one day before day $t$. For our choice of estuarine boundary, a non-linear regression finds that the coefficients $a$, $b$, and $c$ are 0.78, 21.0, and -.152, respectively, with a goodness of fit of $R^2 = 0.93$. We next define an equilibrium relationship between $X_2$ and $Q$ by recognizing that during equilibrium conditions, the position of the $X_2$ isohaline at time $t$ and ($t$-1) are equal. This yields:

$$X_2 = dQ^c, \tag{S2.3}$$

where $d = b/(1-a) = 95$. The fit to Eq. S2.3, as well as a scatterplot of $X_2$ vs. $Q$, is shown in Fig. S2.2b. By substituting Eq. S2.3 into Eq. S2.1, we find an equilibrium relationship between freshwater discharge and the longitudinal salinity profile. This is used to generate Table 1 in the main text.

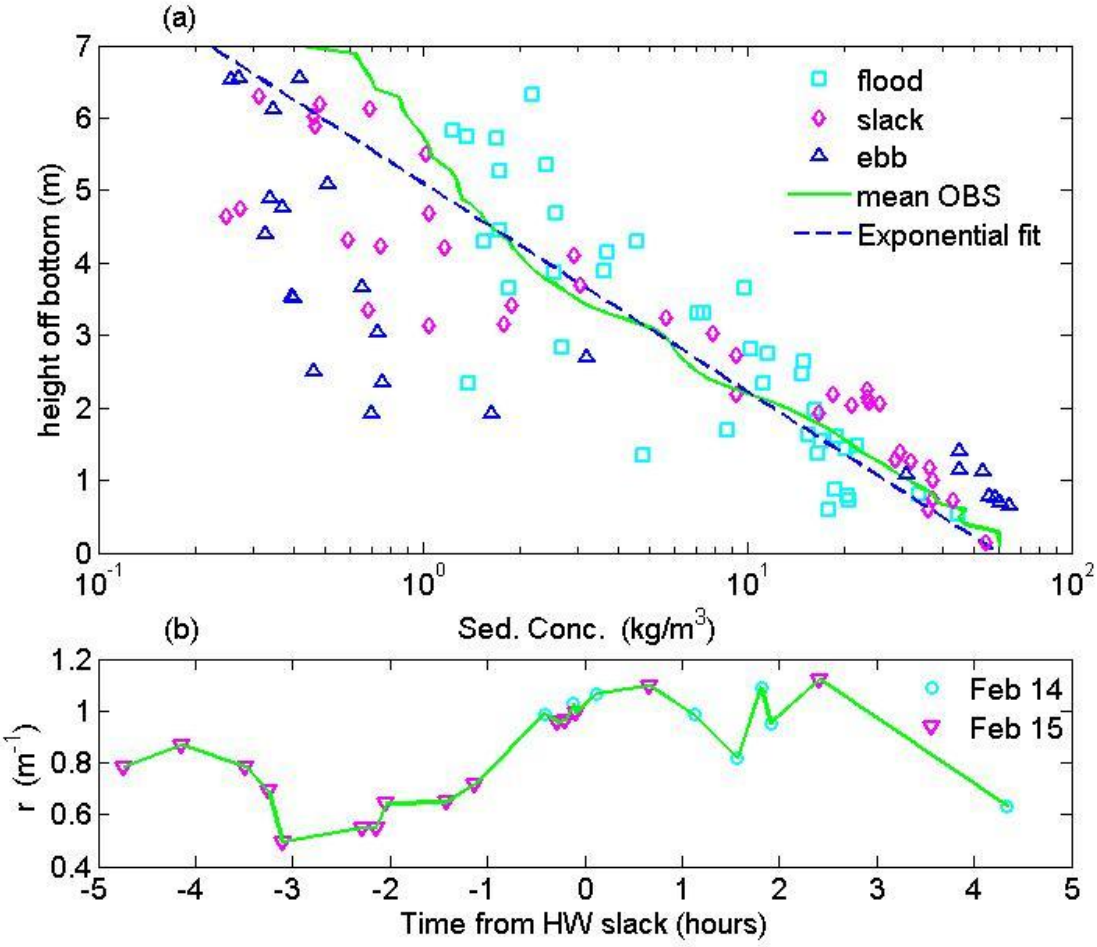


Figure S2.1: Vertical distribution of SSC (a) and the tidal variation of the exponential fitting parameter $r$ [$m^{-1}$] (b) found from 21 OBS/CTD casts and 103 water samples on Feb. 14$^{th}$ and Feb. 15$^{th}$, 2006. Water samples collected during the flood, slack period, and ebb are denoted by squares, diamonds, and triangles, respectively. High-Water Slack lags High Water by ~ 30 minutes. The average of 21 Optical Backscatter profiles (green solid line) and an exponential fit with $r$ = 0.8 (dashed blue line) is shown in (a). This figure is reprinted from Talke et al., 2009.

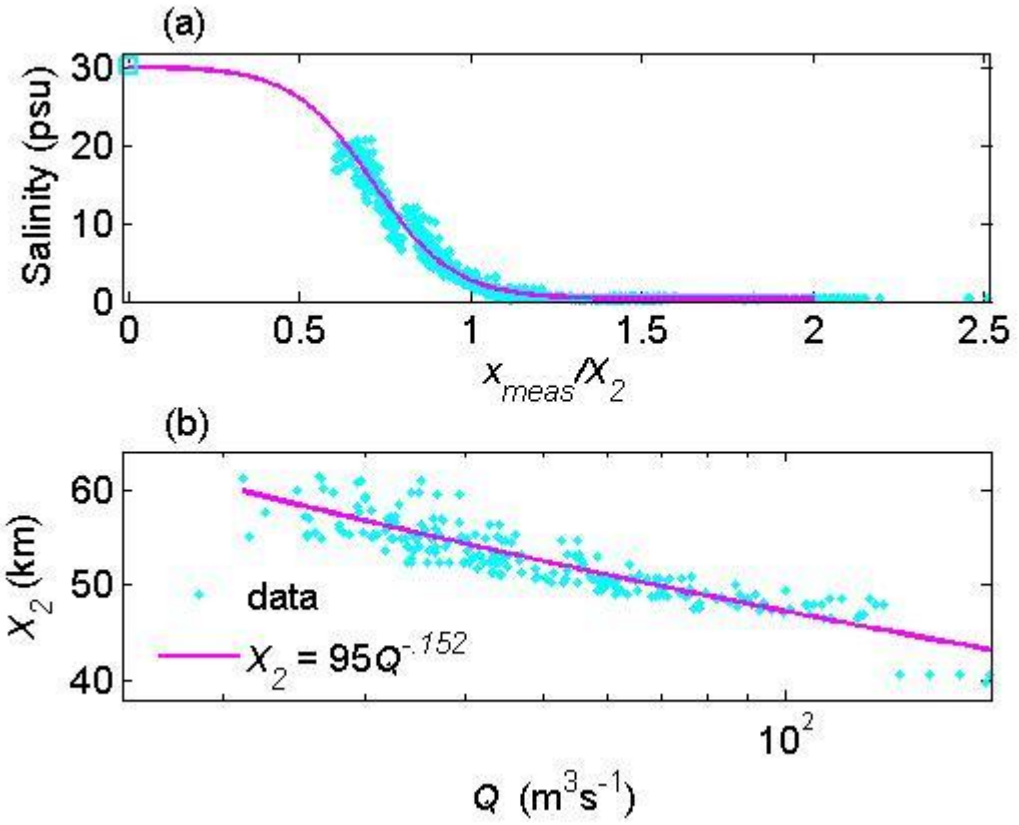


Figure S2.2: Scatter plot of salinity as a function of the normalized coordinate $x/X_2$, (a) and a scatter plot of the $X_2$ isohaline with discharge $Q$ (b). A hyperbolic tangent is fit to the salinity data in (a), while the equilibrium relationship between $Q$ and $X_2$ is given in (b).

# An idealized model and systematic process study of oxygen depletion in highly turbid estuaries

S.A. Talke[1], H.E. de Swart[2], V.N.de Jonge[3]

(1): Civil & Environmental Engineering Department, University of Washington
201 More Hall, Box 352700
Seattle, WA 98195-2700 USA
e-mail: stalke@u.washington.edu

(2): Institute for Marine and Atmospheric research, Utrecht University,
Princetonplein 5, 3584 CC Utrecht, the Netherlands
e-mail: h.e.deswart@uu.nl

(3): Institute of Estuarine Coastal Studies (IECS), University of Hull
Hull, HU6 7RX, United Kingdom
e-mail: v.n.de.jonge@planet.nl

## Supplement S.3: Sensitivity studies of the vertical and estuarine DO model

The dissolved oxygen (DO) model presented in the main text can be analyzed using a full advection-diffusion equation (Eq. 13) which uses inputs from the circulation and morpodynamic model described in Eqs. 1-9, or can be can be simplified to consider vertical balances only. In this supplement we present full sensitivity studies of the vertical and estuarine DO model. These sensitivity studies provide insights into the processes that create or ameliorate hypoxic conditions and describe the fundamentally non-linear response of both SSCs and DO in an estuary to small changes in parameters.

## Vertical DO Model Sensitivity Studies

Figure S3.1 presents the sensitivity of dissolved oxygen (DO) to variations in the water-column averaged SSC ($c_{*d}$) (a), bottom oxygen demand $S_b$ (b), depth $H$ (c), settling velocity $w_s$ of

sediment (d), surface re-aeration coefficient $k_L$ (e), organic decay coefficient $k_r$ (f), eddy diffusivity $K_v$ (g), and temperature $T$ (h), with other parameters held constant to the standard parameters described in Table 2. To estimate the individual oxygen demand of the bed only (b), we set $c_{*d} = 0$ in case (b). For cases c-h, the sensitivity of each parameter is depicted for three different values of $c_{*d}$: $c_1 = 1.0$ kgm$^{-3}$, $c_2 = 2.5$ kgm$^{-3}$ and $c_3 = 5$ kgm$^{-3}$. The envelope of oxygen concentrations throughout the water column is depicted, with a wider band indicating greater difference between the surface (maximum) and bottom (minimum) DO concentrations.

Fig. S3.1 shows that DO concentrations decrease as the total organic material in the water column (proportional to $c_{*d}$) increases or as either the rate of oxygen uptake in the water column ($k_r$) or at the bed ($S_b$) is magnified. As temperature ($T$) increases, DO concentrations plummet due to both greater organic decay ($k_r$) and a reduced oxygen saturation condition, which reduces the total DO available for consumption and limits aeration (proportional to $O_{2,sat} - O_{2,z=0}$). Greater depth results in decreased DO, while increased aeration ($k_L$) causes DO to rise at both the water surface and bed. More mixing ($K_v$) in the water column raises DO at the bed. Only the settling velocity of sediment has a negligible effect on DO. For all parameter studies, increasing the depth-averaged SSC ($c_{*d}$) causes greater oxygen depletion. The magnitude of increased oxygen depletion is nonlinear over each parameter range (see Fig. S3.1c-Fig. S3.1h), with a weak dependence occurring at nearly saturated and nearly anoxic conditions, and a strong dependence observed at intermediate DO concentrations. Changing the depth-averaged SSC shifts the range of parameter values which produce the intermediate (most sensitive) condition.

The difference between top to bottom concentrations of DO are observed to increase as $c_{*d,}$ $H$, $k_r$, and $S_b$ increase, though the differences are less than 1 mg l$^{-1}$over most of the observed parameter space. A negligible difference between top to bottom concentrations of DO are observed for variations in $k_L$ and $w_s$. Only for small values of mixing $K_v$ do top to bottom differences of more than 2 mg l$^{-1}$occur, and surface DO concentrations actually increase. Physically, oxygen poor water near the bed does not diffuse through the water column during poorly mixed conditions

(small $K_v$). Since mixing in the water column decreases strongly as sediment induced stratification increases, river waters with high SSC are likely to see vertical variation in DO (as can be observed in Fig. 2 and Fig. 3 of the main text).

At the surface, the depletion of oxygen depends on the ratio of oxygenation (as parameterized by $k_L$) to the oxygen demand from the bottom boundary ($S_b$) and the total organic matter in the water column ($-pK_r c_{avg} H$). As shown in Eqs. 18-19 of the main text and Fig. S3.1, increases in bed DO demand ($S_b$), organic decay coefficient ($k_r$), average sediment concentration $c_{*d}$ and depth $H$ cause a nearly linear decrease in oxygen concentration. By contrast, the oxygen deficit is inversely proportional to the aeration coefficient ($k_L$); a doubling of the aeration coefficient leads to a halving of the surface oxygen deficit (Fig.S3.1e).

Near the bed, the depletion of oxygen depends on the same parameters as at the surface but also shows a functional dependence on mixing ($K_v$) and on the settling velocity of sediment ($w_s$). However, for the particles considered here, the term $k_L / w_s$ is <<1. Consequently, there is negligible change in DO concentrations as settling velocity is varied in Fig. S3.1d. Similarly, the term $H\, k_L / K_v$, which we term the aeration Peclet number, is much smaller than one for much of parameter range modelled in Fig. S3.1. In this situation, the dissolved oxygen concentration at the bed and surface are identical and do not vary as mixing changes (for example, see the case of $K_v$ = 0.001 $m^2/s$ in Fig. S3.1b). However, as mixing becomes small (i.e., approaches $10^{-4}$ $m^2 s^{-1}$), $H/K_v$ becomes significant compared to $1/k_L$. As a result, bottom and surface concentrations of DO diverge and the bed becomes significantly less oxic than the surface (see Fig. S3.1b).

By subtracting Eq. 18 from Eq. 19 in the main text, we find the top to bottom difference in DO, under the idealized conditions of a constant decay rate $k_r$ (no correction at small oxygen concentrations) and a sediment Peclet number >> 1:

$$\Delta O_2 \approx \frac{S_b H}{K_v} + pk_r c_{*d} H\left\{\frac{-1}{w_s} + \frac{H}{K_v}\right\}. \quad \text{(S3.1)}$$

Hence, the difference between the surface and bottom DO concentration depends both on the bed oxygen demand, $S_b$ and on the decay rate $k_r$ of the total organic material in the water column, $pc_{*d}H$. As sediment is concentrated closer to the bed (due to an increase in the ratio $H/K_v$ for a constant settling velocity), the difference between surface and bed DO concentrations is magnified. Interestingly, aeration has no effect on modelled oxygen differences. Under the condition that $Pe_v >> 1$, the factor $1/w_s$ is smaller than the ratio $H/K_v$, and has little effect on the oxygen differences. In this situation, the difference in DO concentrations due to SSC is inversely proportional to mixing $K_v$ and nearly proportional to $H^2$.

## Estuarine DO Model Sensitivity Studies

A comparison between sensitivity studies of SSC and DO (Figs. S3.2, S3.3 and S3.4) shows, for a wide range of parameter values, that the factors which alter the distribution of SSC dominate the variation in DO. In each figure, the longitudinal profile of depth and width averaged SSC is displayed on the left column, and the DO concentration at the bed ($z = -H$) is depicted on the right column. Each subplot shows the default condition (solid, magenta (dark) line) and the perturbation caused by increasing or decreasing one parameter. For the case of varying discharge $Q$ (Fig. S3.3a and S3.3b) the salinity field (Eq. 3 in the main text) is varied according to a best-fit of available long-term data (see Table 1 of the main text and Supplement S2).

Fig. S3.2a shows that increasing sediment supply ($c_*$) increases the spread and magnitude of depth-averaged SSC, while the location of the estuary turbidity maximum (ETM) remains the same. Similarly, DO concentrations plummet as the sediment supply is increased, and the zone

of stressed (< 5 mg $l^{-1}$) and hypoxic (< 2 mg $l^{-1}$) conditions becomes larger (Fig. S3.2b). Increasing depth moves the turbidity maximum upstream and amplifies SSC; correspondingly, oxygen draw-down intensifies and the zone of depletion becomes larger and moves upstream (Fig. S3.2c and S3.2d). A doubling of depth (from 5 m to 10 m) moves the system from well oxygenated to hypoxic over nearly 40 km. By contrast, increased mixing (eddy viscosity and eddy diffusivity) causes a downstream movement in the ETM, and hence decreased SSC and increased DO concentrations (Fig. S3.2e and S3.2f). The downstream movement occurs because sediment is distributed higher in the water column (increased $K_v$) and because baroclinic circulation decreases (increased $A_v$).

Figs. S3.3a and S3.3b show that as freshwater discharge $Q$ increases, both the ETM and the DO-minimum move downstream. The longitudinal spread of SSC and $O_2$ is decreased, while smaller SSCs result in increased DO concentrations. Greater freshwater discharge increases the downstream flux of sediment, and moves the location of the salt wedge downstream (see Table 1 of the main text). The resulting downstream shift in the turbidity zone also reduces the cross-sectionally averaged SSC (greater width), and thus the oxygen demand from organic material.

Fig. S3.3c shows that increasing longitudinal dispersion produces larger spread of turbidity around the maximum, while decreasing SSC. Similarly, Fig. S3.3d shows spatially circumscribed, intense oxygen depletion for small dispersion ($K_h$ = 25 $m^2s^{-1}$), and a more spread, less intense depletion for large dispersion ($K_h$ = 500 $m^2s^{-1}$). For all cases, the spatial spread of elevated SSC and depleted oxygen are similar, and the location of the SSC maxima and DO minima are nearly identical (the location of the turbidity maximum is independent of $K_h$, since $dc_b/dx$ and hence dispersive fluxes vanish at a maxima, and the morphodynamic balance occurs between freshwater discharge and gravitational circulation). Thus, even for large values of dispersion ($K_h$ = 500 $m^2s^{-1}$), the zeroth order balance of $O_2$ is set by the distribution of SSC, and longitudinal advection and dispersion are higher order effects. Hence, the distribution of DO can

be approximated as a vertical balance (Eq. 16 in the main text), and the processes described in section 4.1 of the main text and in Fig. S3.1 control the modelled oxygen depletion.

Fig. S3.3e and S3.3f show that both large (e.g., 0.006 m $s^{-1}$) and small (0.0002 m $s^{-1}$) values of settling velocity result in relatively small SSCs and a well oxygenated model domain. In between, the maximum SSCs and minimum DO concentrations are observed for a settling velocity of ~ 0.001 m $s^{-1}$. For small settling velocity, sediment is distributed higher in the water column (smaller sediment Peclet number, $Pe_v = w_s H/K_v$) and the ETM is located downstream. The resulting smaller SSCs produce little oxygen depletion. As settling velocity increases, sediment is concentrated closer to the bed, which moves the ETM upstream and reduces the longitudinal spread of turbidity around the maximum. The resulting amplified SSCs cause DO concentrations to decline. However, above 0.001 m $s^{-1}$, the longitudinal spread of the turbidity increases and SSCs decrease, resulting in more oxygenated conditions. The minimum in longitudinal spread of SSC versus settling velocity (and hence the deepest oxygen deficits) occurs because of a minimum in the transport ratio $T_K/T_S$ at a sediment Peclet number of $Pe_v$ ~ 5.9, which occurs just above $w_s$ ~ 0.0008 m $s^{-1}$ for our standard parameters (see Talke et al., 2008).

The effect of changing the salinity field and the geometry of the model estuary are investigated in Fig. S3.4. Upstream intrusion of the salt field (increased $x_c$) moves the ETM upstream and amplifies SSCs, hence producing greater oxygen depletion (Fig S3.4a and S3.4b). Increasing the salinity gradient (decreasing $x_l$) moves the toe of the salt wedge ($x_L + x_c$) downstream and causes downstream migration of the ETM and DO minimum (Fig. S3.4c and S3.4d). Simultaneously, the greater salinity gradient results in greater near-bed (baroclinic) circulation, and compresses the downstream extent of elevated SSC and depleted DO (i.e., increases magnitude of $dc_b/dx$ and $\partial O_2/\partial x$ ). The maximum SSC and minimum DO remain nearly constant.

Changing the width convergence from large (more channel like, larger $L_e$) to small (more funnel shaped, smaller $L_e$) causes a downstream migration of the ETM and DO minimum, and amplifies SSC while decreasing DO concentrations (Fig S3.4e and S3.4f). The downstream movement of sediment occurs because sediment fluxes from freshwater discharge are increased as width becomes smaller at any given $x$ location, while the flux induced by baroclinic circulation remains constant. However, the absolute width at which sediment fluxes from freshwater discharge and baroclinic circulation balance is decreased, causing increased SSC and decreased DO.

Adjusting the width of the estuary mouth ($B_o$) causes similar changes to the balance between SSC fluxes due to freshwater discharge and baroclinic circulation (Fig. S3.4g and S3.4h). As width $B_o$ is increased, SSC fluxes from freshwater discharge (inversely proportional to width) decrease at every location $x$, causing upstream movement of the ETM and DO minimum. SSCs are slightly increased, and DO minimum slightly decreased, because the upstream boundary constrains upstream movement of sediment and amplifies SSCs.

Next we investigate the parameter dependence of two characteristic features of the longitudinal profile of DO: the global minimum in DO in the along channel direction (Fig. S3.5) and the longitudinal spread of the zone of oxygen depletion (Fig. S3.6). Results show that the near bed, minimum DO concentration in the along-channel direction decreases as sediment supply $c_*$ and depth $H$ increase, or as freshwater discharge $Q$, dispersion $K_h$, and mixing $K_v$ decrease (Fig. S3.5). These parameter changes amplify SSC and organic material concentrations at the ETM, causing greater oxygen depletion (Eqs. 18-19 of the main text) and producing greater differences between surface and bed values of DO (Eq. S3.1).

At the surface, the parameters $H$ and $K_v$ produce minima in dissolved oxygen at $H \sim 11$ m and $K_v \sim 0.0008$ m$^2$ s$^{-1}$. For smaller $H$ or greater $K_v$, the maximum SSC is less and DO concentrations are higher. Greater values of $H$ and lesser values of $K_v$ increasingly limit aeration to the upper water column, leading to increased DO near the surface and greater depletion near the bed (see also Fig. S3.1). The parameter study of $w_s$ (Fig. S3.5) shows a DO minimum at ~ 0.001 m s$^{-1}$ both at the surface and bed, which occurs because smaller SSC is observed for both lower and higher values of settling velocity (because of a downstream movement in the ETM

and a larger spread around ETM, respectively; see Fig. S3.3). Because the water column model (Fig. S3.1) predicts little change in DO with settling velocity, the observed change in oxygen depletion is driven primarily by the sediment dynamics.

As salinity is translated upstream ($x_c$ increases), the minimum in DO concentration generally decreases because of upstream movement and amplification of the ETM. As $x_L$ decreases, the salinity gradient steepens and produces greater SSC (due to reduced spread) and a decreasing DO minimum (Fig. S3.5h). For gentle salinity gradients (large $x_L$), the SSC downstream of the ETM becomes more spread, and overall values drop.

The spread of DO concentration below the threshold of 5 mg $l^{-1}$ (which is the concentration below which aquatic organisms are stressed) and below 2 mg $l^{-1}$ (the threshold for hypoxic conditions) are shown in Fig. S3.6. In the simplest cases, the maximum size of the stressed and hypoxic zones corresponds with the parameter value that maximizes SSC and minimizes DO concentrations. Hence, decreased $Q$ and increased $c_*$ result in larger turbidity zones and greater zones of depleted DO. Similarly, the diminished SSCs and hence oxygen demand observed for both small and large settling velocities produces both a minimum DO estimate and maximum depleted zone at an intermediate value of $w_s \sim 0.001$ m $s^{-1}$ (see Fig. S.3.5e and Fig. S3.6e). The behaviour of depth, eddy viscosity, and longitudinal dispersion are more complex (Fig. S3.6). For example, increasing dispersion from $K_h$ =25 $m^2$ $s^{-1}$ to $K_h$ = 100 $m^2$ $s^{-1}$ causes an increased spread of turbidity and hence a greater zone of oxygen stressed conditions (< 5 mg $l^{-1}$), even though the magnitude of the minimum DO concentration has increased. As dispersion is further increased, SSCs become spread over the model domain in such a way that the oxygen concentrations increasingly remain above the 5 mg l-1 threshold. Hence, the size of the depleted oxygen zone decreases. The decrease in the stressed DO zone at large depths ($H$> 11 m) and small mixing ($K_v$ <= 0.0004 $m^2$ $s^{-1}$) occurs because the ETM becomes compressed at the upstream model boundary and the spread of turbidity is decreased.

Fig. S3.6 also shows the non-linear coupling between the size of the depleted oxygen zone and the distribution of SSC. Depending on the starting value, incremental changes in SSC supply (Fig. S3.6a), depth (Fig. S3.6c), discharge (Fig. S3.6b) or eddy diffusivity (Fig. S3.6f), can either greatly increase the zone of oxygen depletion, or have no effect. This variable sensitivity to changing conditions occurs because of the complex relationship between the location of the ETM and the longitudinal spread of SSC for different parameter combinations. For example, increasing depth from 5 m to 8 m causes an upstream migration in the ETM, a 10-fold spike in SSC and organic matter, and produces ~40 km and ~55 km of hypoxic and stressed oxygen zones, respectively (Fig. S3.6c). However, an additional increase to 11 m, while doubling SSC concentrations, changes the zone little because the zone of elevated SSC changes little and the DO demand at 8 m depth already produces a large depleted zone. Though these results are particular to the parameters chosen for the sensitivity study, they nonetheless show the complexity and non-linearity of the processes which create zones of depleted oxygen.

**Figures, Supplement S.3**

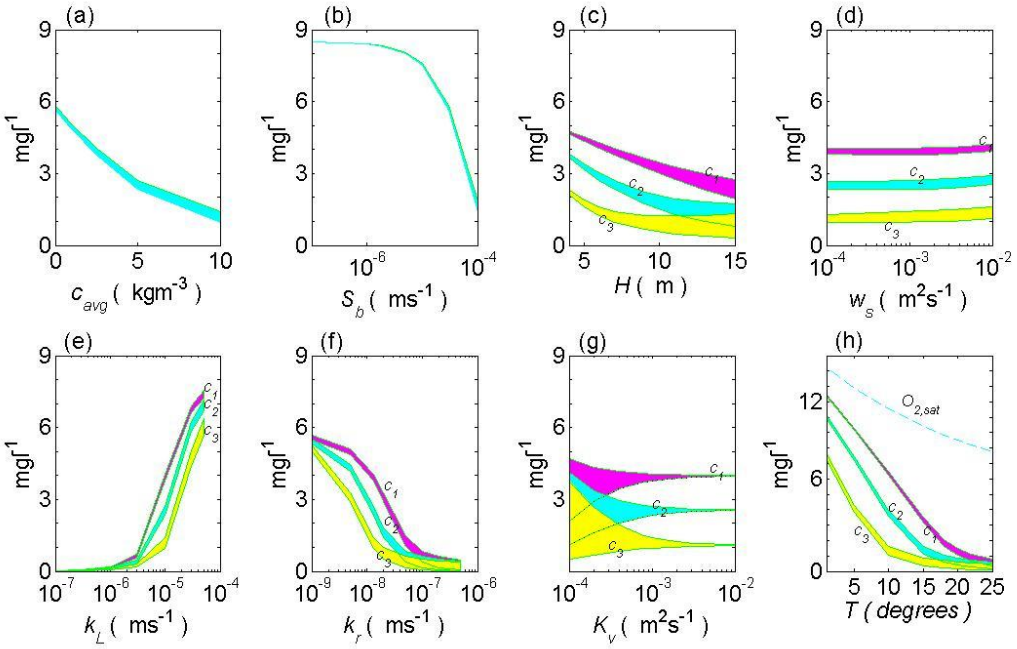


Fig. S3.1: Envelope of dissolved oxygen concentrations in the vertical-only DO model as a function of depth-averaged sediment concentration $c_{*d}$ (a), bottom oxygen demand $S_b$ (b), depth $H$ (c), settling velocity $w_s$ (d), reaeration coefficient $k_L$ (e), organic decay coefficient $k_r$ (f), eddy viscosity $K_v$ (g) and temperature $T$ (h). As a parameter is varied, all other parameters are held at default values found in Table 2 of the main text. Case $c_1$, $c_2$ and $c_3$ refer to sensitivity studies with depth averaged concentrations of 1.0 kgm$^{-3}$, 2.5 kgm$^{-3}$, and 5.0 kgm$^{-3}$. The range of DO concentrations for a set of parameters is depicted by a shaded line, with the maximum occurring at the surface and the minimum at the bed. The dashed line in (g) refers to the minimum DO concentration of case $c_1$ and $c_2$. In (b), $c_{*d}$ is set to zero.

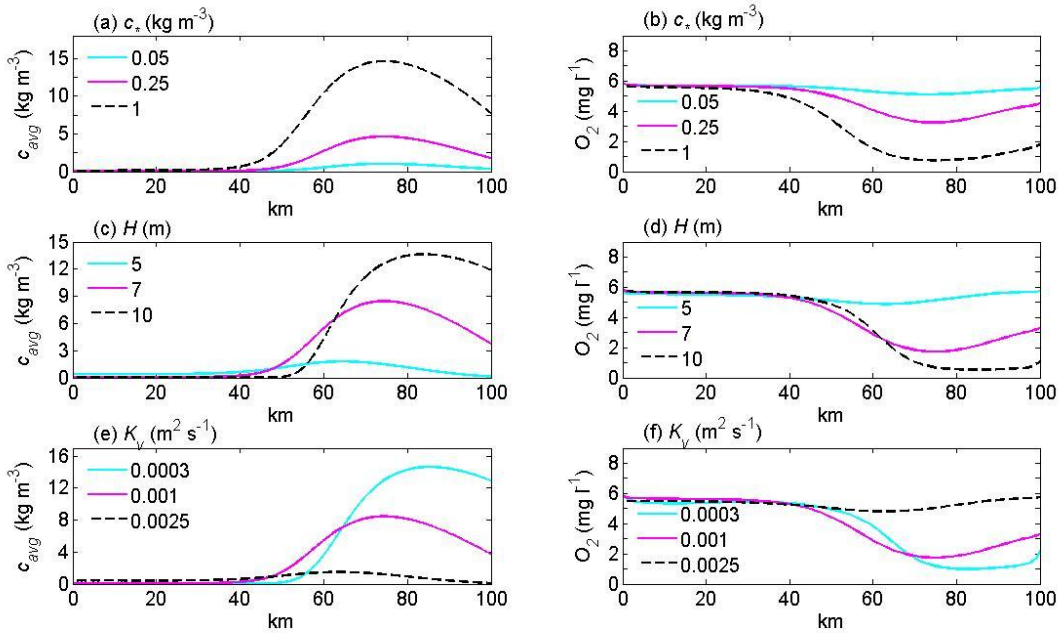


Fig. S3.2: Sensitivity in the modeled longitudinal profile of cross-sectionally averaged SSC (a, c and e) and bottom ($z$ = -$H$) DO concentration (b, d, and e) to variations in prescribed, estuary-averaged SSC $c_*$ (a and b), depth $H$ (c and d) and eddy diffusivity $K_v$ (e and f). In the model, eddy viscosity and eddy diffusivity are held equal to each other. Default values are used for all other parameters (Tables 1-3 of the main text).

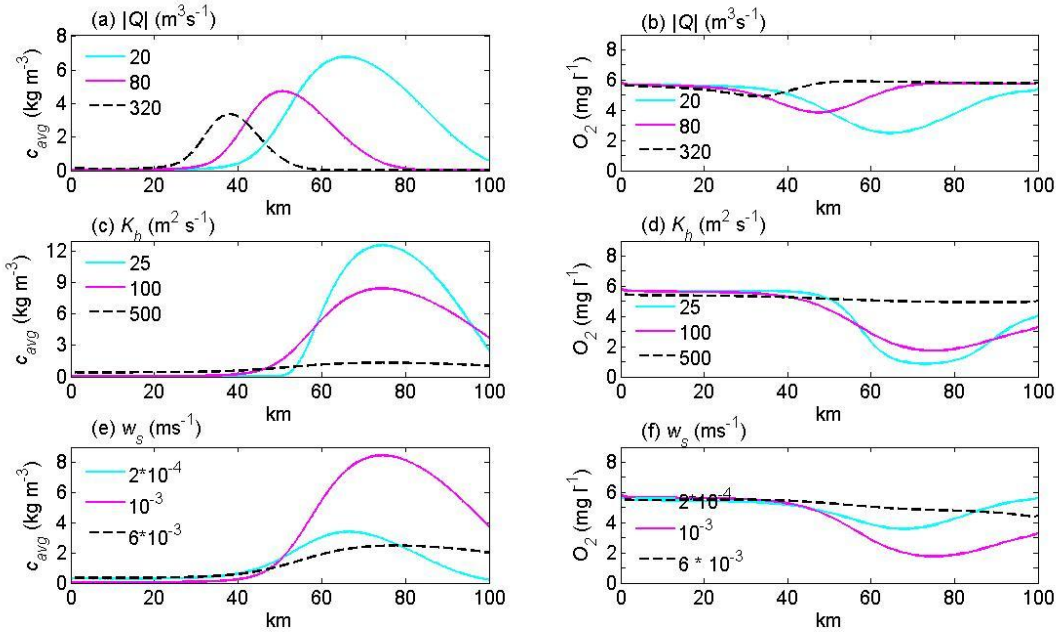


Fig. S3.3: Sensitivity in the modeled longitudinal profile of cross-sectionally averaged SSC (a, c and e) and bottom ($z$ = -$H$) DO concentration (b, d, and e) to prescribed variations in freshwater discharge $Q$ (a and b), longitudinal dispersion $K_h$ (c and d) and settling velocity $K_v$ (e and f). Default values are used for all other parameters (Table 1-3).

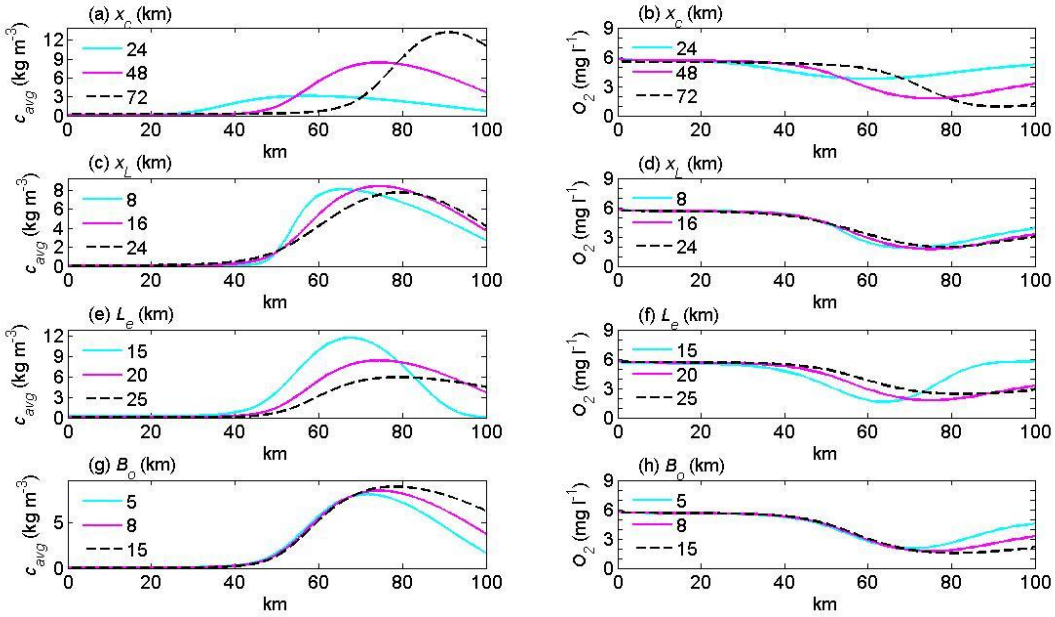


Fig. S3.4: Sensitivity in the modeled longitudinal profile of cross-sectionally averaged SSC (a, c, e, and g) and bottom ($z$ = -$H$) DO concentration (b, d, e, and h) to prescribed variations in the location of the maximum salinity gradient $x_c$ (a and b), length scale of over which salinity varies $x_L$ (c and d), convergence length-scale of the estuary $L_e$ (e and f), and width Bo at the seaward boundary ($x$ = 0 ) of the estuary (g and h) . Default values are used for all other parameters (Table 1-3).

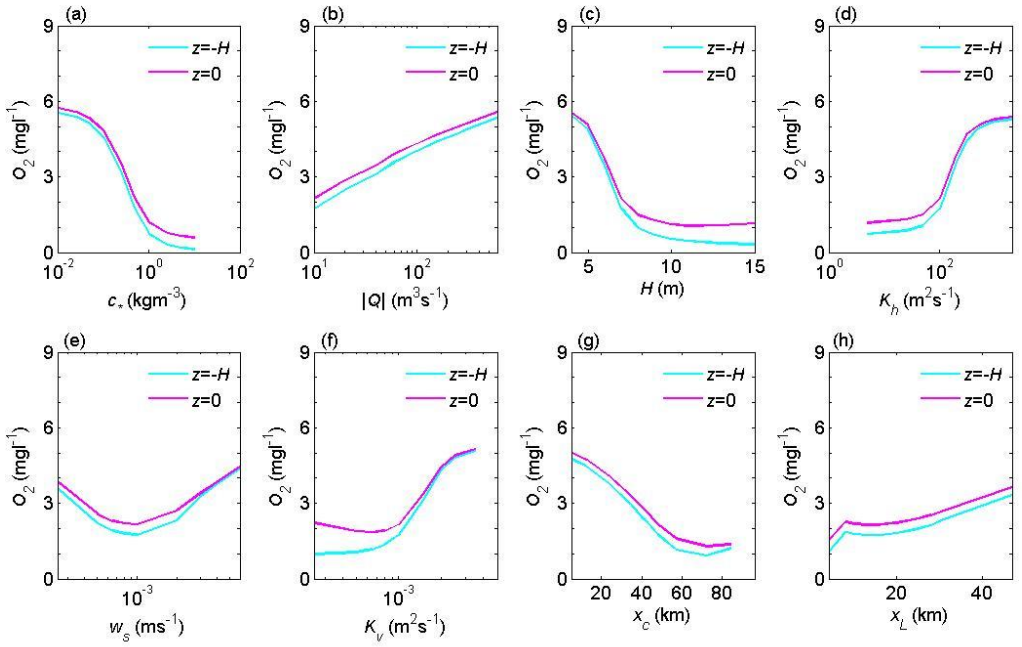


S3.5: Variation in the modeled minimum of longitudinal DO concentrations at the bed ($z = -H$) and at the surface ($z = 0$) as a function of average concentration $c_*$ (a), freshwater discharge $Q$ (b), depth $H$ (c), dispersion $K_h$ (d), settling velocity $w_s$ (e), mixing $K_v$ (f), location of maximum salinity gradient $x_c$ (g), and the length scale of the salinity gradient $x_L$(h).

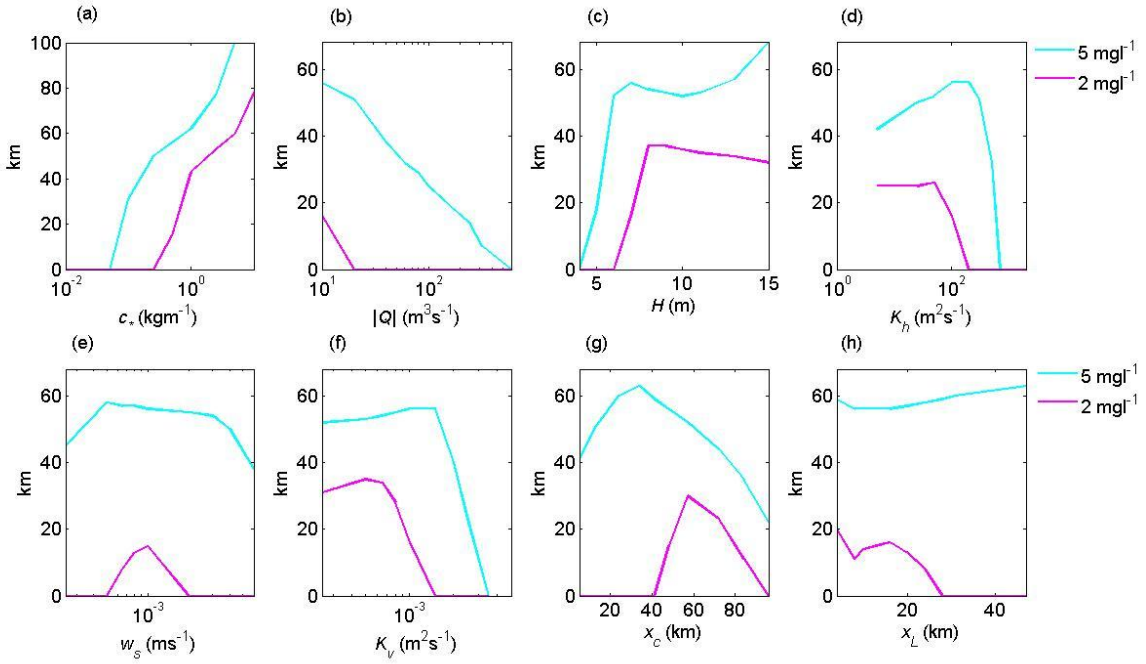


S3.6: The spread of the hypoxic zone vs. model parameters, as measured by the longitudinal distance over which the bottom ($z$ = -$H$) concentration of DO is below either 5 mg l$^{-1}$ or 2 mg l$^{-1}$. The model parameters are: average concentration $c_*$ (a), freshwater discharge $Q$ (b), depth $H$ (c), dispersion $K_h$ (d), settling velocity $w_s$ (e), mixing $K_v$ (f), location of maximum salinity gradient $x_c$ (g), and the length scale of the salinity gradient $x_L$(h).